Czech University of Life Sciences Prague

Faculty of Environmental Sciences

Department of Water Resources and
Environmental Modelling

Diploma Thesis

Development and sensitivity analysis of hydrodynamic model for a tidal channel in an urban area. Case study: Guayaquil city

Julio Enrique Torres Monroy

March 2023

CZECH UNIVERSITY OF LIFE SCIENCES PRAGUE

Faculty of Environmental Sciences

DIPLOMA THESIS TOPIC

Author of thesis:	Eng. Julio Torres, BSc
Study programme:	Environmental Modelling
Thesis supervisor:	Ing. Luděk Bureš, Ph.D.
Supervising department:	Department of Water Resources and Environmental Modeling
Language of a thesis:	English
Thesis title:	**Development and sensitivity analysis of hydrodynamic model for a tidal channel in an urban area. Case study: Guayaquil city**
Objectives of thesis:	Development of hydrodynamic model based on the obtained data. Sensitivity analysis of physical and computational parameters.
Methodology:	1. Data collection: DEM, flow network, land use, hydrological data. 2. Hydrological analysis based on precipitation data 3. Creating of hydrodynamic model. 4. Sensitivity analysis.
The proposed extent of the thesis:	60 p
Keywords:	Hydrodynamic, Numerical Model, HECRAS, Sensitivity analysis

Recommended information sources:

1. HEC-RAS 2D User's Manual. Hydrologic Engineering Center [online]. Copyright © 2022 USACE Hydrologic Engineering Center [cit. 30.04.2022]. Dostupné z: https://www.hec.usace.army.mil/confluence/rasdocs/r2dum/latest
2. Matej Vojtek, Andrea Petroselli, Jana Vojteková, Shahla Asgharinia; Flood inundation mapping in small and ungauged basins: sensitivity analysis using the EBA4SUB and HEC-RAS modeling approach. Hydrology Research 1 August 2019; 50 (4): 1002–1019. doi: https://doi.org/10.2166/nh.2019.163
3. SINGH, V P. *Computer models of watershed hydrology*. Colorado: Water Resources Publications, 2012. ISBN 978-188720174-2.
4. Te Chow, V. (1959). Open-channel hydraulics (Vol. 1). New York: McGraw-Hill.

Expected date of thesis defence:	2022/23 SS - FES

Electronically approved: 31. 3. 2023
prof. Ing. Martin Hanel, Ph.D.
Head of department

Electronically approved: 31. 3. 2023
prof. RNDr. Vladimír Bejček, CSc.
Dean

Author's Statement

Hereby declare that I have independently elaborated the diploma thesis with the topic of: **Development and sensitivity analysis of hydrodynamic model for a tidal channel in an urban area. Case study: Guayaquil city** and that I have cited all the information sources that I used in the thesis and that are also listed at the end of the thesis in the list of used information sources.

I am aware that my diploma thesis is subject to Act No. 121/2000 Coll., on copyright, on rights related to copyright and on amendment of some acts, as amended by later regulations, particularly the provisions of Section 35(3) of the act on the use of the thesis.

I am aware that by submitting the diploma thesis I agree with its publication under Act No. 111/1998 Coll., on universities and on the change and amendments of some acts, as amended, regardless of the result of its defence.

With my own signature, I also declare that the electronic version is identical to the printed version and the data stated in the thesis has been processed in relation to the GDPR.

Julio Enrique Torres Monroy

Acknowledgement

A special thanks to my thesis supervisor Bureš Luděk, for his time, support and good questions.

To my colleagues at CADS-ESPOL who guided me and provided the data in a timely manner.

To Maria Esther who has been with me throughout my master's degree and more, and without a doubt to my family, thanks to whom all this would not be possible.

Julio Torres

Abstract

Natural hazards, primarily floods, affect the worldwide population's daily life, and their impacts have been well studied from different edges. Estuaries and coastal areas are of vital importance in the lives of human beings, especially those who live in their vicinity. However, these ecosystems have been degraded yearly with an accelerated loss. In delta cities such as Guayaquil, tidal channels are significant natural assets that help society in many ways. Hence, hydrodynamic models must be developed and used to comprehend the intricate interplay between natural and artificial forces and create efficient management methods. In this context, the current study focuses on the hydrodynamic modelling of branch A of the Estero Salado in Guayaquil, Ecuador. Moreover, A set of 18 scenarios were simulated in order to get a clear picture of how the hydrodynamic model of channel A in the Salado estuary would react to changes in boundary conditions, hydraulic roughness, and time step. This sensitivity analysis aims to show how sensitive the model's outputs are to changes in an input variable, analyzing two parameters, the maximum water surface elevation and the flood area. In addition, the combination of the worst boundary condition was found. The results revealed that the system could collapse when the channel faces high tide levels and the peak of the hydrograph. Additionally, the boundary conditions greatly impacted the model results, having a difference of more than 25% in reservoir levels and more than 80% in the flood area (between a 2-year event and another 100-year event). However, this significant difference was not seen when the hydraulic roughness was analyzed, having only differences even less than 1%. Finally, the computation time analysis showed clear signs that 1 minute is sufficient to maintain stability in the model and obtain optimal results (without error carryover) in a relatively low computation time. The study concludes that the canal will overflow in extreme precipitation that coincides with high tide, affecting the surrounding houses. It also makes clear ideas for improvement and future analysis that allow deepening the study of the estuarine ecosystem.

Contents

1 Introduction

Natural hazards affect the daily life of the worldwide population and their impacts have been well study from different edges (Easterling et al., 2012; Kharb et al., 2022). It is to be expected that flood threats will grow more and more, not only in frequency but also in magnitude, impacting directly to the vulnerable population; in that sense, it is crucial to do a correct analysis in order to associate the risk in urban areas (Johnson et al., 2016; Kvočka et al., 2016; Lechowska, 2018). There are various actions that can be taken to lessen flood damage, each of which has a basis in logic and is crucial to flood defense. The implementation of traditional flood protection systems is still crucial, but flood prevention and flood risk management should take on a bigger role (Vojtek & Vojteková, 2016).

Estuaries and coastal areas are of vital importance in the lives of human beings, especially those who live in their vicinity. However, these ecosystems have been degraded year by year (Lotze et al., 2006) with an accelerated loss of tree species natives that already had more than 35% degradation of mangroves at the beginning of the 21st century (cite) having a direct impact on its hydrodynamic behaviour (Valiela et al., 2001). In delta cities such as Guayaquil, estuaries are held up as a natural remedy as storm-driven coastal flooding rises as a result of climate change (Fairchild et al., 2021). Tidal channels are significant natural assets that help society in many ways, including transportation, fishing, and recreation. The fact that these channels are frequently found in populated regions means that human activity there has the potential to significantly affect how they behave hydrodynamically. To comprehend the intricate interplay between natural and artificial forces in this situation and to create efficient management methods, hydrodynamic models must be developed and put to use.

The current study focuses on hydrodynamic modeling of an Ecuadorian city's tidal canal. Since Guayaquil is a coastal city with a sizable population and a sizable economy, managing its natural resources sustainably and preventing flooding are difficult tasks. The research area is the branch A of the Estero Salado, a major component of the region's hydrological cycle that runs through the city's heart.

Six sections make up this report, plus an appendix with a seventh section. A brief introduction to the flood overview and hydrodynamic models is provided in Section 1. The technique utilized to carry out the study is outlined in Section 2, along with the data used for pre-processing, hydrological analysis, hydrodynamic modelling, and sensitivity analysis, as well as the tools employed for the analysis. The results are discussed in Section 3, which also highlights the patterns associated with two important variables: the maximum water surface level (WSL) in the reservoir and the flooded area. Section 4 conducts a thorough analysis of the outcomes and comparisons with other studies. With its conclusions, Section 5 wraps up the analysis. The bibliography cited in the thesis is listed in Section 6.

1.1 Objectives

This study aims to develop a numerical model representing the hydrodynamics of a tidal channel in the reach "A" of the Estero Salado estuary in 1 Guayaquil

city - Ecuador. Besides, a sensitivity analysis is performed to identify how the simulation results change over the variability of the physical and computational parameters.

Data collection from different sources is reached to achieve the objectives. Then, a hydrological analysis is carried out to obtain a synthetic storm and extreme values in different return periods, 2, 10, 50 and 100 years. Besides, a worst-case combination analysis, tidal plus hydrograph, is needed to determine the worst condition in the system (high tide level and strong precipitation).

Outputs from the hydrological and tidal analysis are the input for the hydrodynamic model. Moreover, together with the tide control structure, the hydrodynamic model is set up with specialized tools such as HECRAS and geographical information system packages.

2 Methodology

2.1 Study area

Guayaquil is the most populated (2‘644.891) in Ecuador (INEC, 2017), being an economy of trade and industry thanks to one of the main harbours that the country has to the south of the city. Guayaquil is located on the right bank of the Guayas River, which is made up of the Babahoyo and Daule rivers; thus, together with the Gulf of Guayaquil (figure 2.1a-b), form the largest estuarine system on the Pacific Coast of South America (Armijos & Montolío, 2008).

The Gulf of Guayaquil is highly influenced by a major tidal system, which is affected by the El Niño - Southern Oscillation (ENSO) phenomenon bringing unusually warm surface water into the southern Pacific Ocean. This event produces heavy rainfalls from the wet season and can last between 9 months and two years (Barrera Crespo et al., 2019; Reynaud et al., 2018; Twilley et al., 1997). In the upper left corner of the Gulf of Guayaquil is located the Estero Salado, made up of a set of complex channels that cross Guayaquil from the south to the centre-north of the city.

In this study, the first channel upstream of Estero Salado is modelled (Figure 2.1c). Also, this upper natural channel is the so-called reach "A", which begins from Ecomundo school to Urdesa bridge. Therefore, the domain area encloses the drainage basin of this reach with a total area of 13.8 km^2. The Urdesa Bridge connects the Urdesa and Kennedy neighbours, and in 2021, the Guayaquil Municipality built a tidal control system of 17 valves: 15 pinch type and two check type (figure 2.2).

The pinch valves have a mechanism that allows to close the flow from both direction upstream to downstream and vice versa when the tide level reaches 1.5 m AMSL. Similarly, the check valves allow the flow to go just from upstream to downstream. Therefore, the tidal control structure blocks the flow from downstream to upstream when high tide levels is coming; thus, the reach "A" can store water while a rainfall event is done.

2.2 Data

The data used in this project was collected from several sources, both public and private institutes. Many of them, such as precipitation, were used to do the hydrological analysis before the hydrodynamic simulation; others, like the digital elevation model, were used to perform the hydrological and hydrodynamic models.

It is essential to highlight that most of the data came in different formats and resolutions, so prepossessing work was needed to refine the data and make it suitable for analysis. This work is described in the following sections.

2.2.1 Precipitation

The Oceanographic and Antarctic Institute of Ecuador (INOCAR) provided the rainfall data from the rainfall station located at the INOCAR offices, approxi-

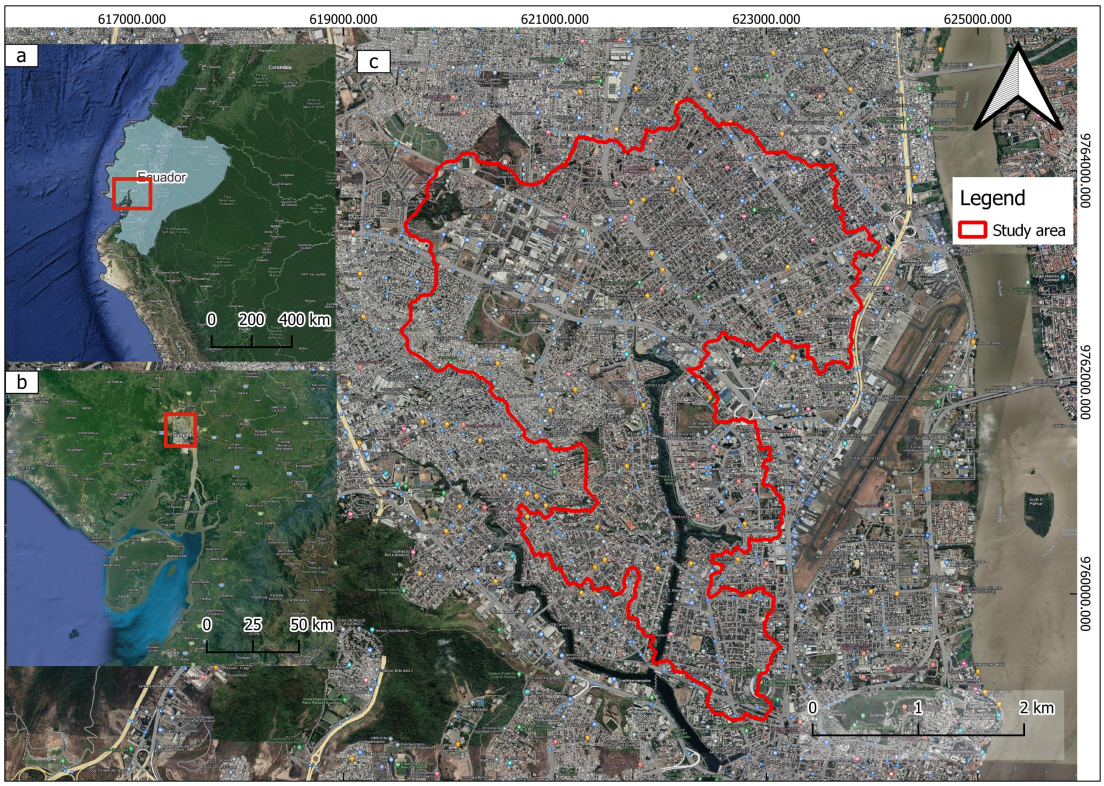

Figure 2.1: a) location of the study area in Ecuador, b) Map of the Salado estuary system and the Guayas river, c) Location of the reach "A" where the red line represent the study domain

Figure 2.2: Photograph of the downstream side of Urdesa bridge and its flood control valves. Photo taken by Luis Dominguez.

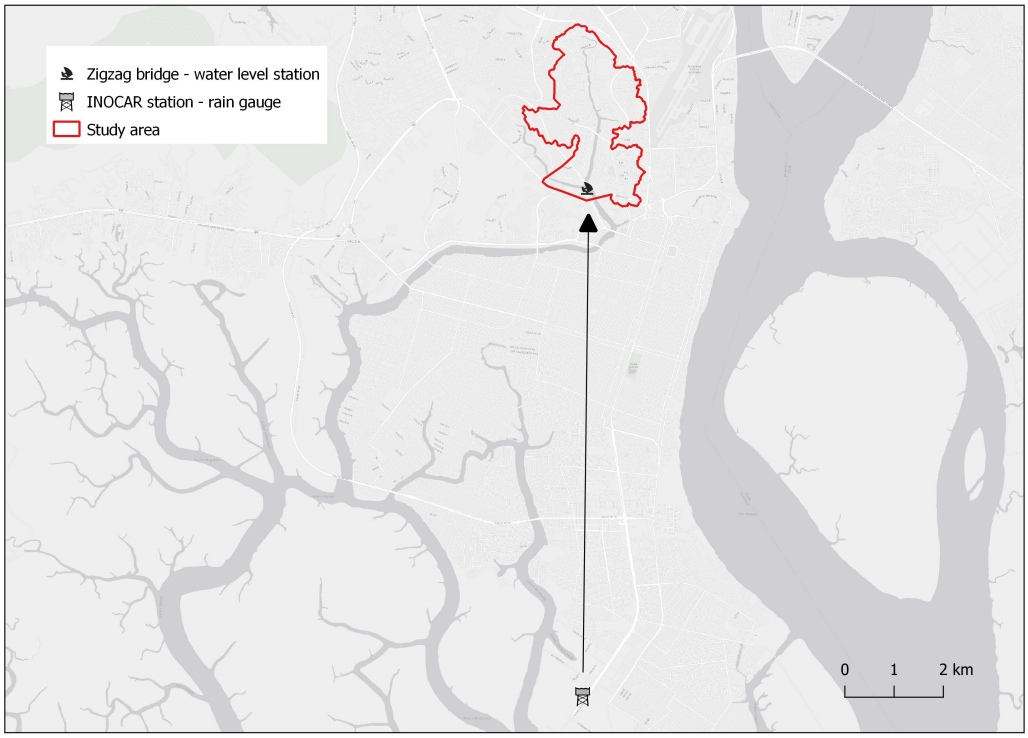

Figure 2.3: Precipitation and tide level stations used in this study

mately 10.5 km from the study site. (Figure 2.3). This data is given in daily resolution from 01/01/1962 to 31/05/2019.

2.2.2 Bathymetry

The bathymetry data was collected by two sources, INOCAR and the Water Municipality Company of Guayaquil - EMAPAG (figure 2.4). These in-situ data were valuable to update the digital elevation model and capture the natural bed surface of the channel. The INOCAR's bathymetry was sampled in the mean lowest water surface (MLWS) and the EMAPAG's bathymetry in AMSL. These different references are a problem when it comes to modelling and analysis since they can get results that are completely wrong from reality. Therefore, to avoid these problems, it is proceeded to convert the data from INOCAR to AMSL.

2.2.3 Digital elevation model

The digital elevation model used in this study is an orthophoto-based image with 5mx5m resolution. This DEM was provided by the Centre from Water and Sustainable Development (CADS) of the ESPOL University. During the preprocessing stage, the bathymetry points from INOCAR and EMAPAG were incorporated into the DEM, having a new DEM with the accurate bed elevation. Figure 2.5 shows the original (5mx5m resolution) DEM and the bathymetry updated DEM used in this study.

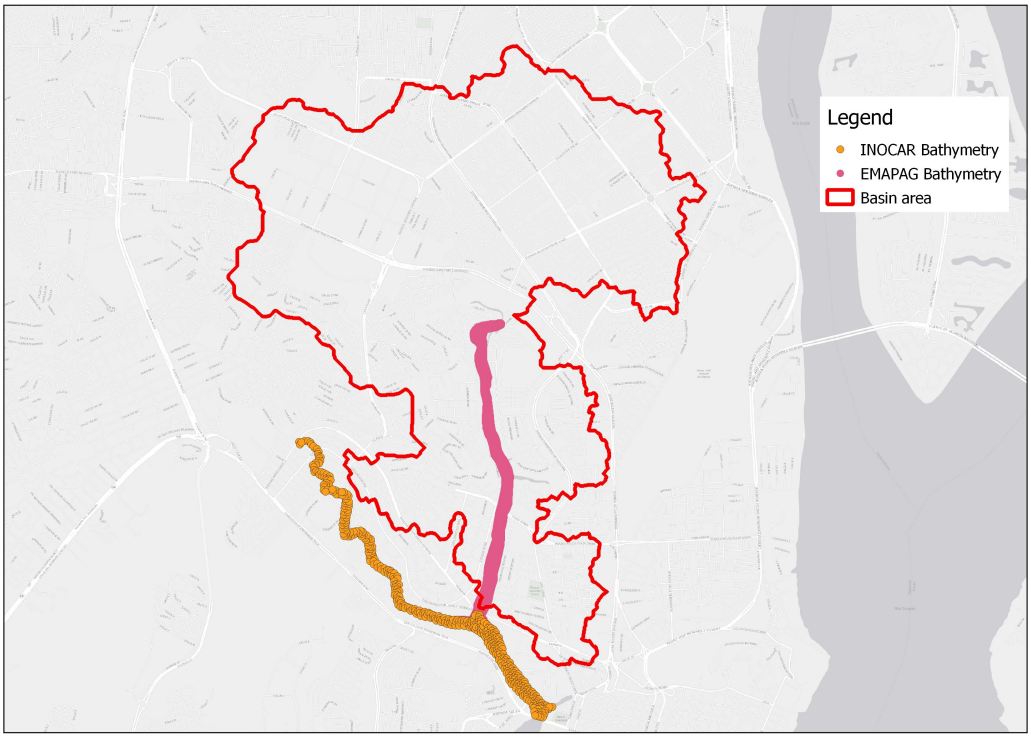

Figure 2.4: Bathymetry points location from EMAPAG (pink) and INOCAR (yellow)

Figure 2.5: Comparison between (left) initial DEM of $5mx5m$ resolution - orthophoto and (right) updated DEM - measured bathymetry

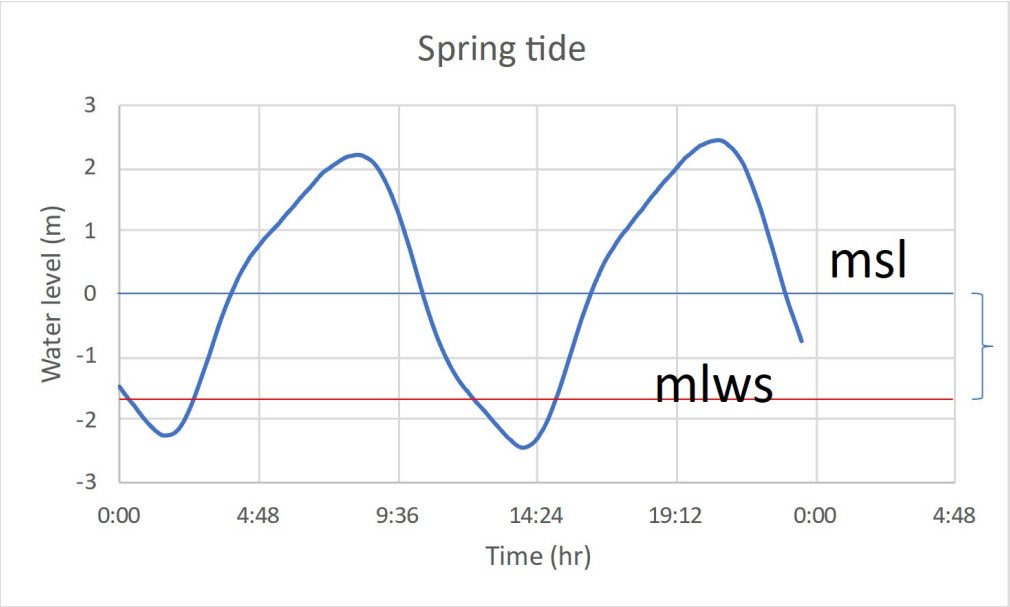

Figure 2.6: Spring tide event registered in Zigzag station. Red line is the mean lowest water surface and blue line is the local mean sea level. Z_0 is the different between msl and mlws.

2.2.4 Water levels

Water levels refer to the tidal from the estuary to the study area. This data was measured from the water level station in the Zigzag bridge located in the domain area downstream (see figure 2.3).

The water level time series was measured for six months, from December to May, in 30-minute intervals (see C). However, this data came originally in the mean lowest water surface (MLWS) reference used for the navy purpose; in that sense, a reference shift was performed by adding the Z_0 value from the bathymetry points (Figure 2.6).

In this study, an event based is simulated; this means that the entire time series is not required in the model. Hence, the maximum tide amplitude in one day (spring tide) was selected to study the worst-case event.

2.3 Hydrological analysis

2.3.1 Drainage area

The hydrological analysis was divided into two areas; the first one represents the drainage area that discharges to the upstream region once a storm event is given, where the hydrograph generated is the upstream boundary condition in the hydrodynamic model. Similarly, the adjacent region from the channel discharges into the reservoir, adding extra water volume to the system; this discharge is represented as uniform lateral flow into the hydrodynamic model (Figure 2.7).

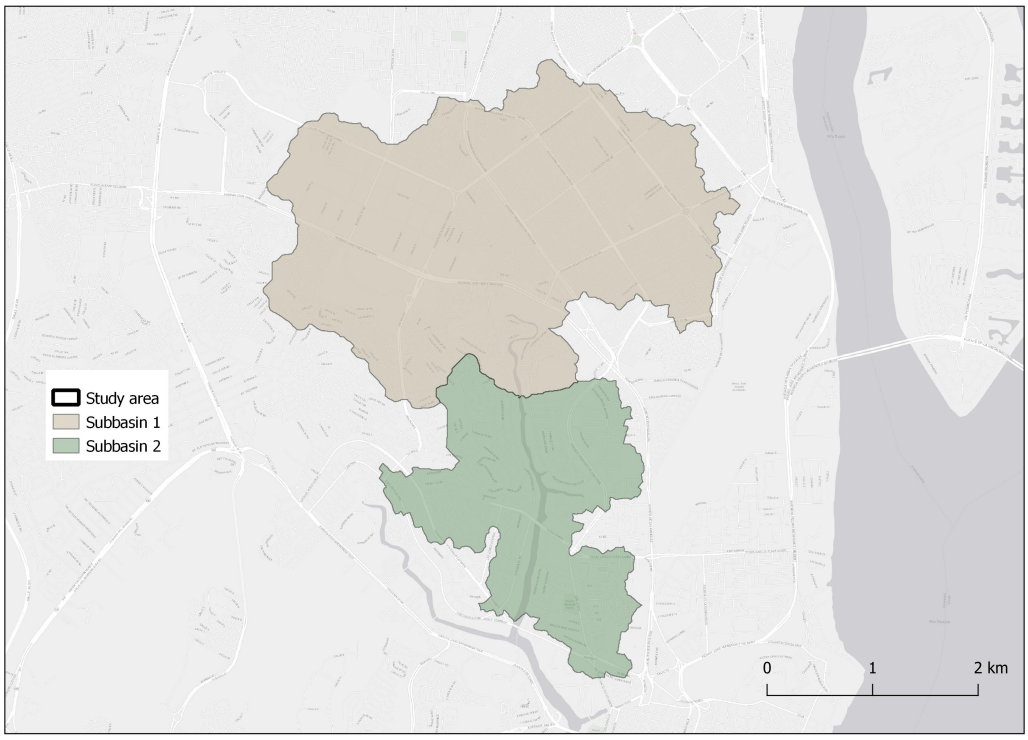

Figure 2.7: Draining area representation for the system. "Sub-basin 1" generates the upstream boundary condition hydrograph. "Sub-basin 2" generates the lateral uniform flow hydrograph.

2.3.2 Maximum analysis

A frequency analysis was carried out to find the relation between extreme events and their occurrence probability (Te Chow et al., 1962). The statistical analysis and the Kolmogorov-Smirnov test (Table 2.1) are performed through the specialised tool "Hydrognomon" which has been applied in several hydrological studies (Garba et al., 2013; Kozanis & Mamassis, 2010).

From the Kolmogorov-Smirnov test, the data best fit to statistic Pearson III (Table 2.1) with a $\delta Max = 0.08558$.

Once the statistics were established, the total precipitation (see: A) for a given time was calculated with the Dick Peschke equation:

$$P_d = P_{24h} * \left(\frac{d}{1440}\right)^{0.5} \quad (1)$$

Table 2.1: Kolmogorov-Smirnov test for Pearson III, LogNormal, Log Pearson III and Gumbel. The Pearson III is highlighted in green to indicate that precipitation data fit better to this statistic.

Kolmogorov-Smirnov test	**a=1%**	**a=5%**	**a=10%**	**DMax**
Pearson III	ACCEPT	ACCEPT	ACCEPT	0.08558
LogNormal	ACCEPT	ACCEPT	ACCEPT	0.09003
Log Pearson III	ACCEPT	ACCEPT	ACCEPT	0.09195
EV1-Max (Gumbel)	ACCEPT	ACCEPT	ACCEPT	0.09429

Where:

P_d = total precipitation [mm]

P_{24h} = 24 hours maximum precipitation [mm]

d = duration [min]

After a lineal regression process, the IDF curve equation was found:

$$I = \frac{971.337 * T^{0.165}}{D^{0.751}} \tag{2}$$

Where:

I = intensity [mm/hr]

T = return period

D = duration [min]

Table 2.2 shows the design precipitation based on the Alterning block method for an event duration of 180 minutes and 2, 5, 10, 25, 50 and 100 years. In the appendix B, the hyetograph is generated by the Alterning block method.

2.3.3 Hydrological modeling - HEC HMS

The HEC HMS model is used to calculate the design hydrographs used in the hydrodynamic model. The U.S. Army Corps of Engineers created this software to simulate the hydrological cycle in American basins (U.S. Army Corps of Engineers, 2012). Hence, HEC-HMS provides a variety of options to simulate rainfall-runoff processes and flow transit, among others (Duque-Sarango et al., 2019). In this study, the hydrological modelling involves three processes: infiltration, rainfall-runoff transformation and the routing method on the reach element.

The infiltration method used in this process is the SCS loss method, which relates land use and soil data to calculate the curve number (CN) of a given basin and thus determine the rate of soil infiltration (R. Kabiri & Bai, 2013). Thus, the landcover map data (Figure 2.8) was collected from the European Space Agency (ESA), which generates a $10mx10m$ resolution product for 2021 based on Sentinel-1 and 2 data.

The ModClark model adapts Clark's unit hydrograph technique to accommodate spatially distributed rainfall data. This model is made up of a linear channel in

Table 2.2: Design storm for 180 minutes event a return period of 2, 5,10, 25, 50 and 100 years

Time (min)	Return Period Precipitation (mm)					
	Tr 2	**Tr 5**	**Tr 10**	**Tr 25**	**Tr 50**	**Tr 100**
0-10	0.98	1.14	1.28	1.49	1.67	1.87
10-20	1.08	1.26	1.41	1.64	1.84	2.06
20-30	1.21	1.40	1.57	1.83	2.05	2.30
30-40	1.38	1.60	1.80	2.09	2.34	2.63
40-50	1.61	1.88	2.10	2.45	2.74	3.08
50-60	1.97	2.30	2.57	3.00	3.36	3.77
60-70	2.61	3.03	3.40	3.95	4.43	4.97
70-80	4.08	4.74	5.32	6.18	6.93	7.78
80-90	32.23	37.49	42.04	48.91	54.84	61.49
90-100	6.08	7.07	7.93	9.23	10.35	11.60
100-110	3.15	3.67	4.11	4.78	5.36	6.01
110-120	2.24	2.60	2.92	3.40	3.81	4.27
120-130	1.77	2.06	2.31	2.69	3.02	3.38
130-140	1.48	1.73	1.94	2.25	2.52	2.83
140-150	1.29	1.50	1.68	1.95	2.19	2.45
150-160	1.14	1.33	1.49	1.73	1.94	2.17
160-170	1.03	1.19	1.34	1.56	1.75	1.96
170-180	0.94	1.09	1.22	1.42	1.60	1.79

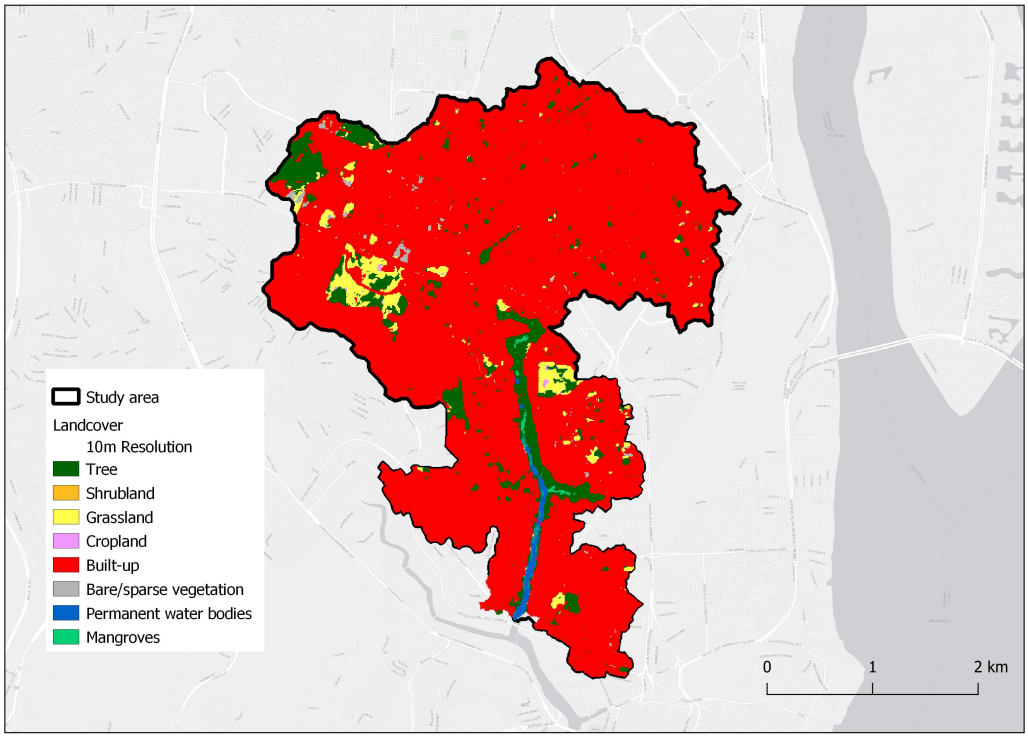

Figure 2.8: Land cover map with 10m resolution for the study area. This information was taken from the European Sapce Agency (ESA).

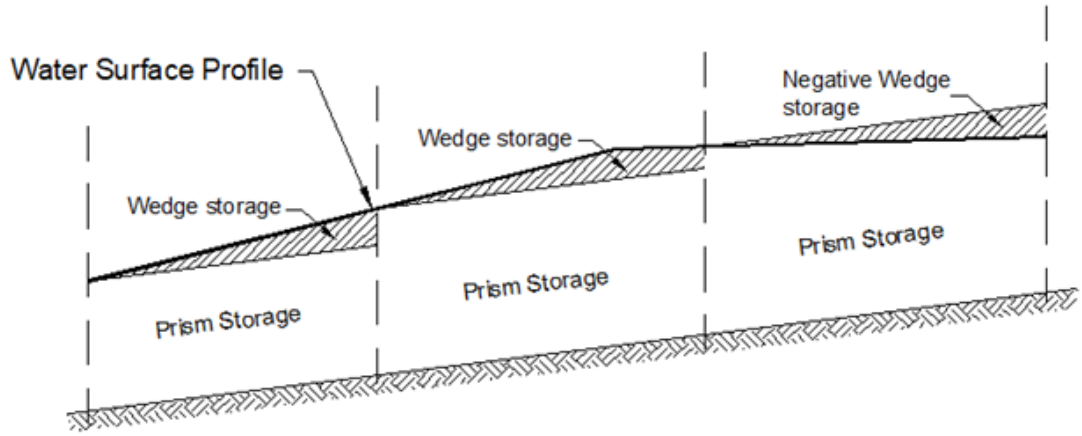

Figure 2.9: Muskingum Representation of Channel Storage, reproduced from Linsley, Kohler, and Paulhus, 1982

series with a linear reservoir whose outflow is the IUH. Additionally, two parameters (eq. 3, 4) are required to compute the Clark model, concentration-time (T_c) and storage coefficient (R) (Bhattacharya et al., 2012).

$$T_c = 2.2 \left(\frac{LxL_C}{\sqrt{S}} \right)^{0.3} \tag{3}$$

T_c = Time concentration [hr]

R = Storage coefficient [hr]

L = Length of the longest watercourse withing the drainage area [mile]

L_C = Stream length to the basin centroid [mile]

S = Average slope of the flow path, represented by 10% to 85% of the longest watercourse [ft/mile]

$$\frac{R}{T_C + R} = 0.5 \tag{4}$$

Applying the conservation of mass law, the Muskingum routing method routes an inflow hydrograph. Thus, This technique can replicate the frequently noticed enhanced channel storage on the rising side of a passing flood wave and decreased channel storage during the falling side. To do this, the conceptualisation of a reach's total storage as the addition of wedge (or triangle) and prism (or rectangle) storage is used (Figure 2.9).

Table 2.3 shows a resume of the hydrological parameters used in this model for both BC and lateral uniform flow hydrograph, where an average CN value of **98** was used to simplify the calculus.

The graphs 2.10 and 2.11 show the discharge over time for return periods of 2, 5, 10, 25, 50, and 100 years. Peak lateral flows range from more than 15 to almost 35 $m^3 3/s$, whereas peak flows upstream range from more than 30 to over 70 m^3/s. To see HEC-HMS outputs, refer to appendix D.

Table 2.3: Hydrological parameters used in the HEC-HMS models for the boundary condition and the lateral uniform flow hydrograph

Hydrological parameters	
Boundary condition	
CN	98
Tc	2.97
R	2.97
Lateral flow	
CN1	98
Tc1	0.964
R1	0.964
CN2	98
Tc2	1.39
R2	1.39
CN3	98
Tc3	1.82
R3	1.82
CN4	98
Tc4	0.358
R4	0.358

2.4 Hydrodynamic Model

2.4.1 HEC-RAS

An integrated software system called HEC-RAS was created for interactive use in a multi-user, multi-tasking network environment. A graphical user interface (GUI), distinct hydraulic analysis components, data storage and administration capabilities, visuals, and reporting tools are all parts of the system.

Four one-dimensional river analysis components are included in the HEC-RAS system: (1) steady flow water surface profile computations, (2) unsteady flow simulation (one-dimensional and two-dimensional hydrodynamics), (3) quasi-unsteady or fully-unsteady flow movable boundary sediment transport computations (1D and 2D), and (4) water quality analysis. The usage of a common geometric data representation and geometric and hydraulic computing procedures by all four components is a crucial component. The system has various hydraulic design elements that can be used after the fundamental water surface profiles have been computed, in addition to the four river analysis components. A comprehensive spatial data integration and mapping system is also part of HEC-RAS (HEC-RAS Mapper).

The conservation of mass (eq. 5) and the concept of conservation of momentum (eq. 6 are the two physical laws that control how water moves through a stream. The continuity and momentum equations, often known as partial differential equations, are the mathematical representations of these rules.

$$\frac{\partial A}{\partial t} + \frac{\partial Q}{\partial x} = q_l \tag{5}$$

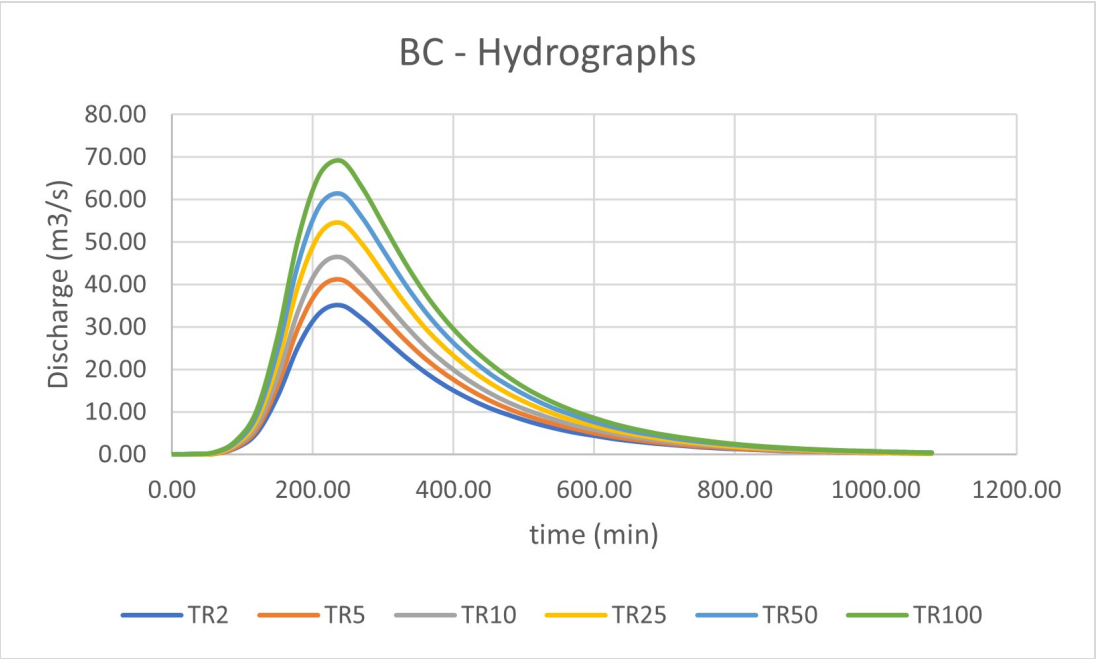

Figure 2.10: Design hydrograph of return periods of 2, 5, 10, 25, 50 and 100 years for boundary condition input.

Where $\frac{\partial Q}{\partial x}$ is the rate of flow in the control volume, $\frac{\partial A}{\partial t}$ is the rate of change in storage and q_l is the lateral inflow per unit length.

$$\frac{\partial Q}{\partial t} + \frac{\partial (vQ)}{\partial x} + gA\left(\frac{\partial Z_s}{\partial x} + S_f\right) = 0 \tag{6}$$

where g is the acceleration of gravity, S_f is the friction slope and V is the velocity.

2.4.2 Model domain

The simulated channel has 51 cross sections (figure 2.12), with an average separation of nearly 50 meters, and is a total of 2439 meters long. There is a flyover with 17 tidal control valves at height 0+232. A tidal time series was established as a downstream boundary condition, and hydrographs were used as an upstream boundary condition.

2.4.3 Cross sections

The cross sections have good hydraulic geometry and range in depth from 4 meters in the upstream direction to 8 meters in the downstream direction on average. They are 50 meters apart from one another on average (figure 2.13). Its length varies between 300 to 400 meters.

2.4.4 Boundary conditions

The numerical model needs the recording of two boundary conditions (upstream and downstream) in order to solve the differential equations that govern the hydrodynamics of the channel. Downstream a tidal time series is established, while upstream a hydrograph is defined.

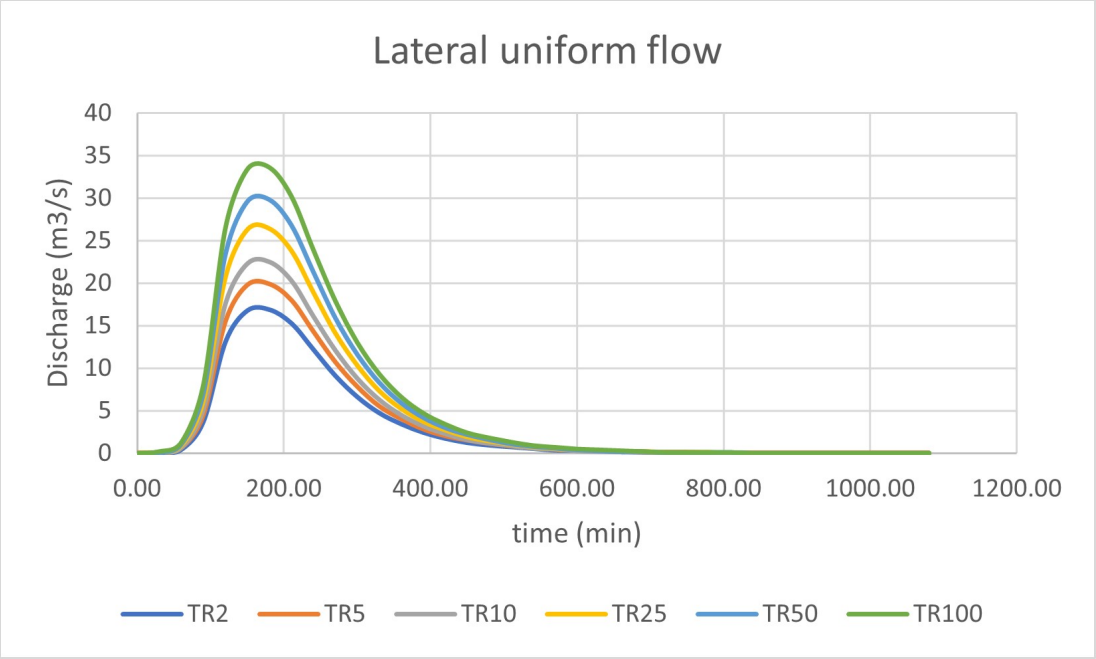

Figure 2.11: Design hydrograph of return periods of 2, 5, 10, 25, 50 and 100 years for lateral uniform flow input.

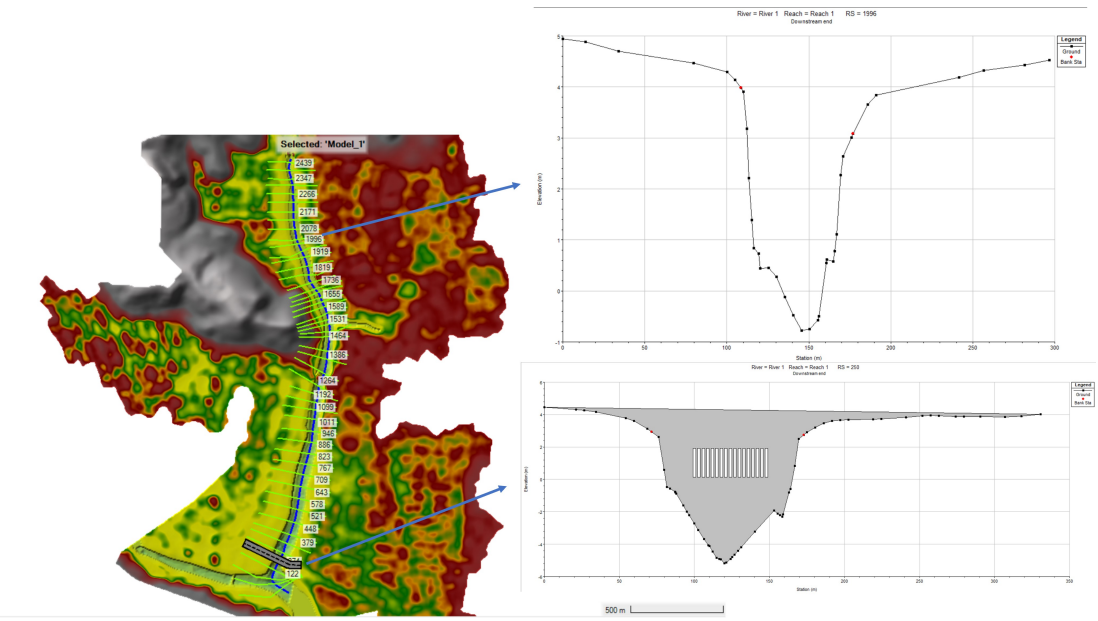

Figure 2.12: Estuary branch A model domain showing a the cross section distribution along the channel and the arrangement of the tidal control valves

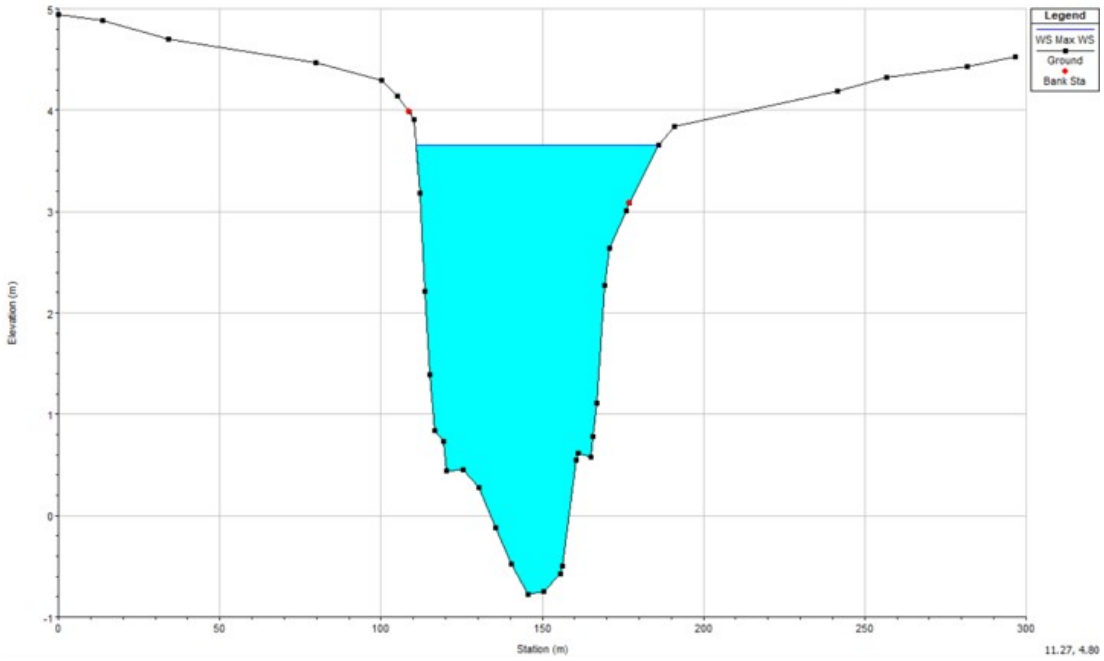

Figure 2.13: Typical cross section configured in the hydrodynamic model

2.4.5 Hydraulic roughness

In order to accurately determine a Manning number that depicts the landscape under study, modellers must be very careful to account for the hydraulic roughness coefficient, an important physical characteristic that links the type of soil and is sensitive to even the smallest changes. The bottom of the channel has some stones, as shown in picture (2.2), which leads us to believe that the roughness coefficient is 0.055, as shown in figure 2.14. The Manning coefficient's base value of 0.12 was chosen because the floodplains are made up of trees or mangroves (figure 2.15).

2.4.6 Tidal control measure

The tidal control system, inaugurated in December 2021, consists of 15 pinch valves and 2 check valves. The pinch valves allow flow from upstream to downstream and vice versa, while the check valves only allow one-dimensional flow from the reservoir into the estuary channel.

HEC-RAS allows the use of gates as valve models, which can be configured according to an event or system condition, but unfortunately the software does not allow the partial closure of the valve set, i.e. all valves must be closed and opened (pinch and check). In this study it has been configured that when the downstream water level reaches 1.5 m AMSL, the valves close at a rate of 0.1 m/min.

2.4.7 Computational parameters

The base numerical model has a modelling time of two days, i.e. it captures 4 high and 4 low tides, as well as 2 hydrograph peaks. In addition, the time step for the calculation is 1 minute and captures results every 10 minutes (figure 2.17).

Table 3-1 Manning's 'n' Values

Type of Channel and Description	Minimum	Normal	Maximum
A. *Natural Streams*			
1. **Main Channels**			
a. Clean, straight, full, no rifts or deep pools	0.025	0.030	0.033
b. Same as above, but more stones and weeds	0.030	0.035	0.040
c. Clean, winding, some pools and shoals	0.033	0.040	0.045
d. Same as above, but some weeds and stones	0.035	0.045	0.050
e. Same as above, lower stages, more ineffective slopes and sections	0.040	0.048	0.055
f. Same as "d" but more stones	0.045	0.050	0.060
g. Sluggish reaches, weedy. deep pools	0.050	0.070	0.080
h. Very weedy reaches, deep pools, or floodways with heavy stands of timber and brush	0.070	0.100	0.150

Figure 2.14: Manning's 'n' values for main channel

d. Trees				
1.	Cleared land with tree stumps, no sprouts	0.030	0.040	0.050
2.	Same as above, but heavy sprouts	0.050	0.060	0.080
3.	Heavy stand of timber, few down trees, little undergrowth, flow below branches	0.080	0.100	0.120
4.	Same as above, but with flow into branches	0.100	0.120	0.160
5.	Dense willows, summer, straight	0.110	0.150	0.200
3. **Mountain Streams, no vegetation in channel, banks usually steep, with trees and brush on banks submerged**				
a.	Bottom: gravels, cobbles, and few boulders	0.030	0.040	0.050
b.	Bottom: cobbles with large boulders	0.040	0.050	0.070

Figure 2.15: Manning's 'n' values for flood plain

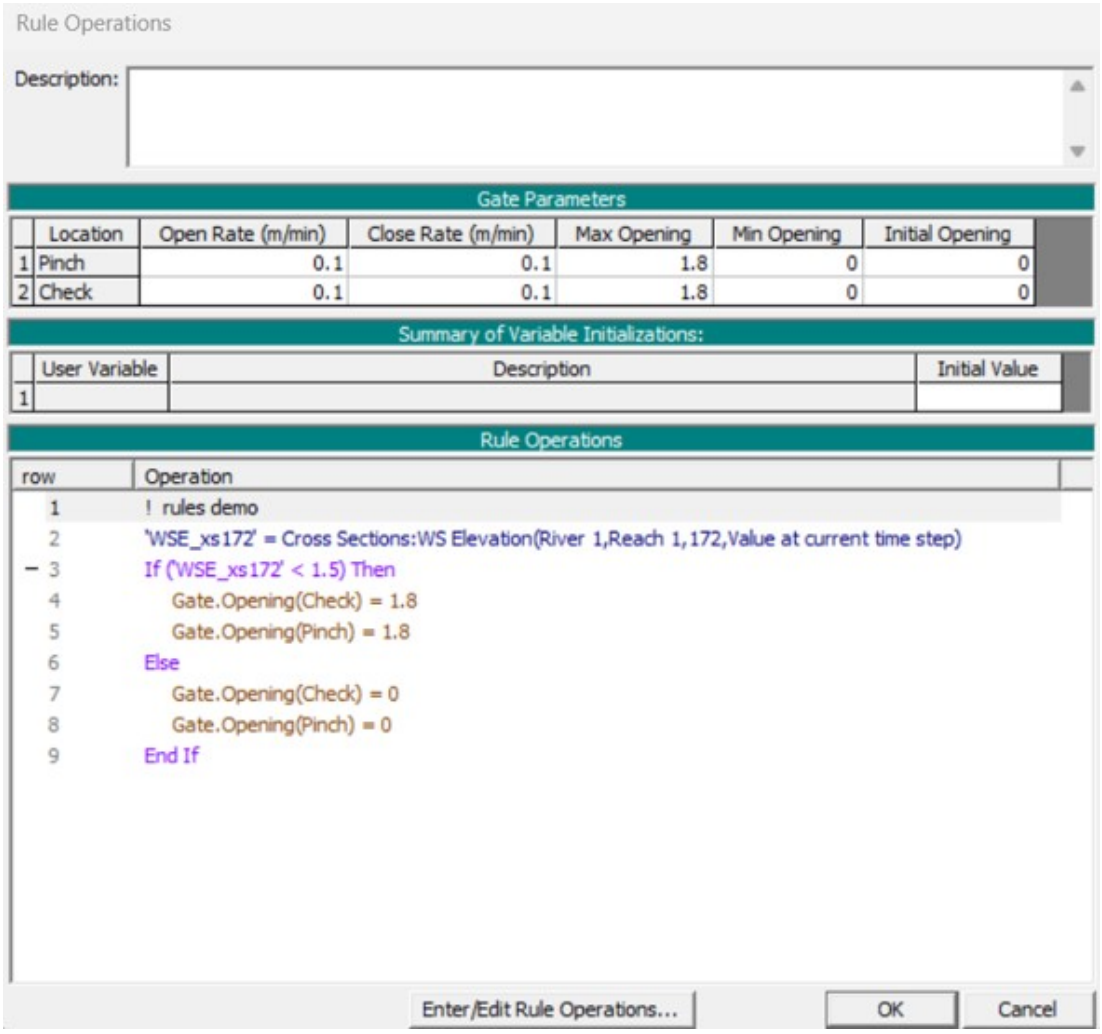

Figure 2.16: Gate configuration scheme in HEC-RAS

Since the numerical model is solved by the finite difference method for non-stationary flows, a parameter theta is used in an interval from 0.6 to 1, where 0.6 implies more accurate but more unstable solutions. In this study a value of 0.6 for theta was used (figure 2.18). Other computational parameters help to improve the stability or play with the errors tolerance in the model, the study of these parameters are outside the scope of this project.

2.5 Sensitivity analysis

A set of 18 scenarios were simulated in order to get a clear picture of how the hydrodynamic model of channel A in the Salado estuary would react to changes in boundary conditions, hydraulic roughness, and time. The purpose of this sensitivity analysis is to show how sensitive the model's outputs are to changes in an input variable.

According to a thorough analysis of the literature (Crespo, 2016; Cunderlik & Simonovic, 2004; Molenaar et al., 2018; Ongdas et al., 2020), it was determined that both physical and computational characteristics have an impact on the outcome and functionality of the numerical model. The simulated scenarios used in

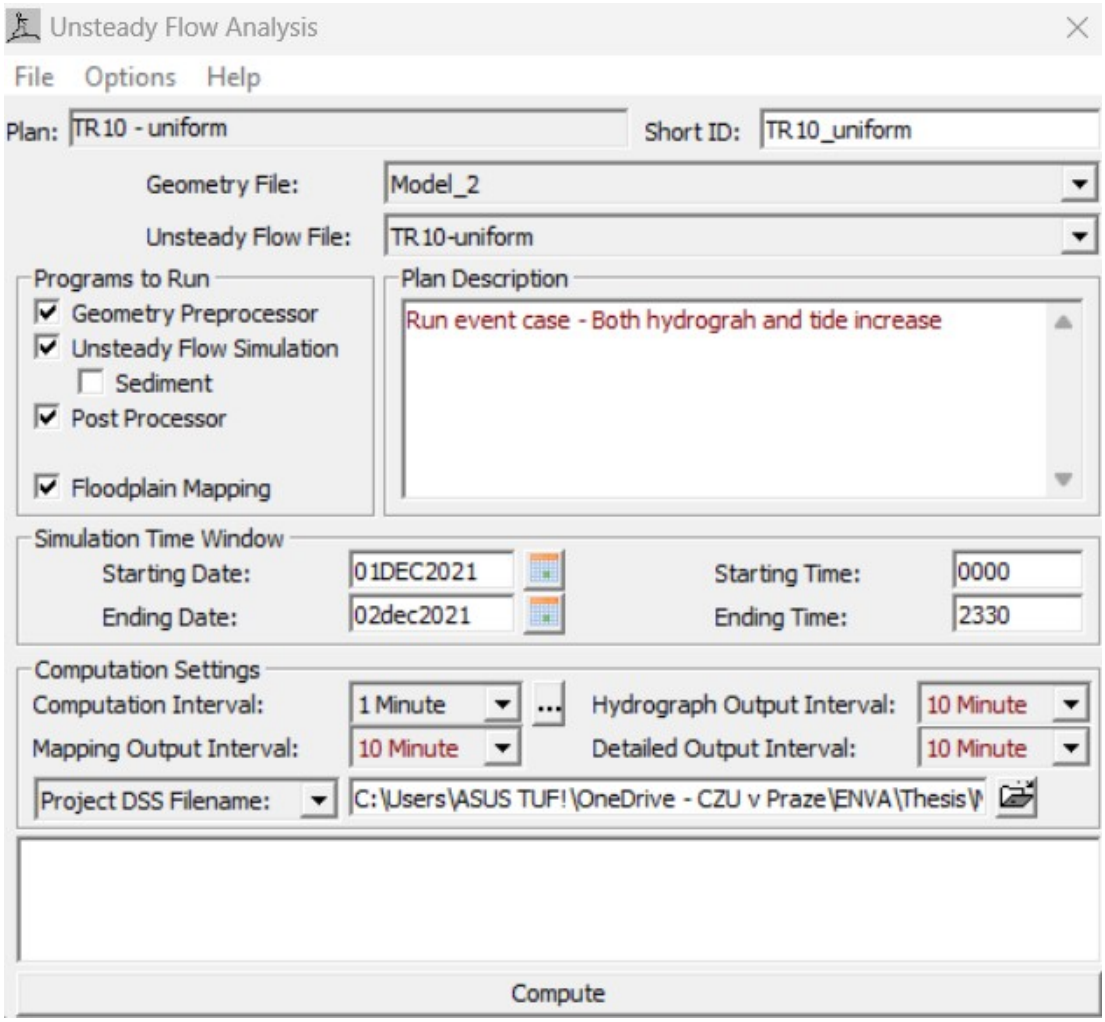

Figure 2.17: Gate configuration scheme in HEC-RAS

this study are organized into three major groupings in Figure 11. The maximum water surface level and the flood area were the variables analyzed.

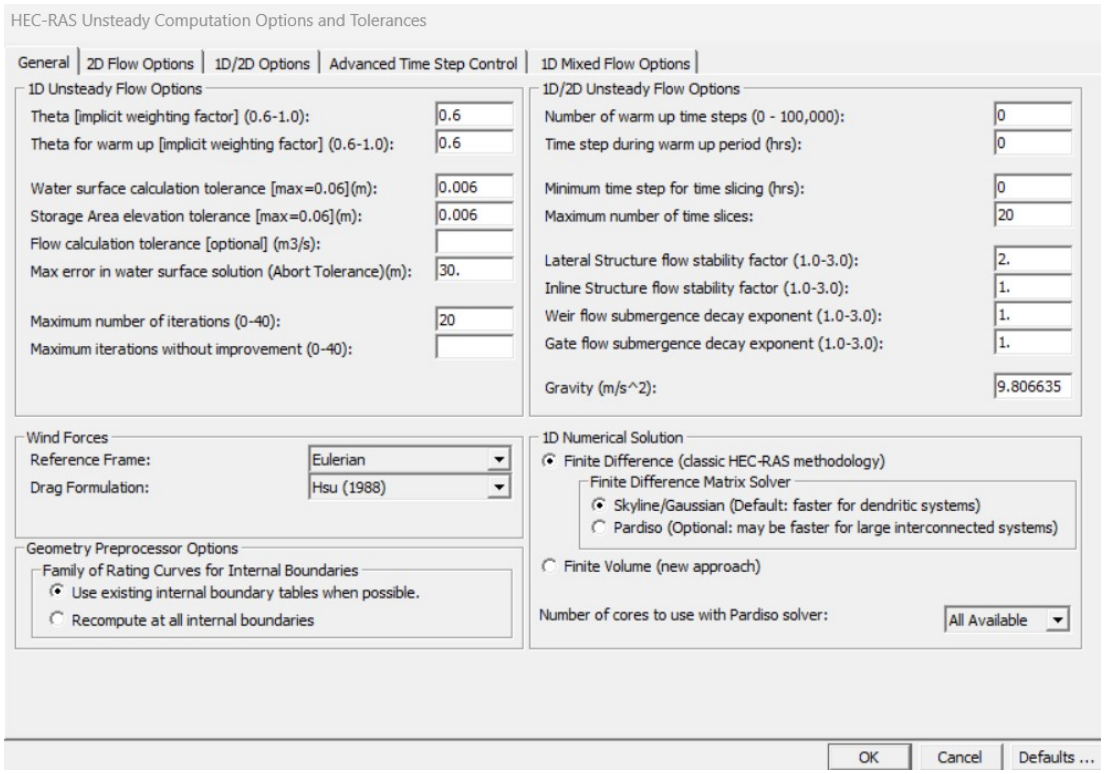

Figure 2.18: Gate configuration scheme in HEC-RAS

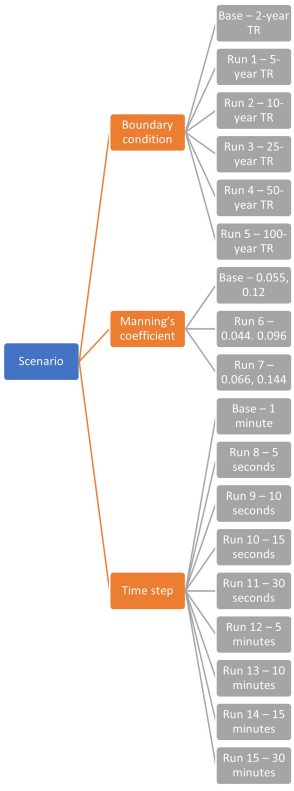

Figure 2.19: Overview of the schematic model scenarios showing the values used for the base model across all categories and the input values set for each simulation

3 Results

3.1 Worst case scenario

3.1.1 Water level

In order to determine the most critical interaction between the tide and the rainfall event, a worst-case scenario analysis was carried out. Therefore, three scenarios were simulated: 1) when the high tidal and peak hydrograph meet, 2) when the lowest water level meets with the peak hydrograph, and 3) when the high tidal meet with no rainfall event. The upstream boundary condition for these scenarios was a ten-years return period hydrograph.

The figures 3.1, 3.2, and 3.3 show the water level just upstream and downstream of the structure, as well as the total flow through the gates over time. It is notable how there are extra high-water levels (3.65m) when the peak flow and tidal meet from the first scenario. The second scenario result (hydrograph increase and tide decrease) shows how the water level increases (until 1.9m) with a peak flow; however, this peak is rapidly attenuated due to the tide decreasing. Similarly, the third scenario result shows that the water level before the gates reaches 2.35m.

3.1.2 Flooded area

Figure 3.4 shows each scenario's flooding extent over the study area. The first scenario floods a total area of 22.16 ha, the second scenario has a flood extent of 15.94 ha, and the third scenario reaches 16.37 ha.

The water level difference between scenarios 1 and 2 is 1.75m, and between scenarios 1 and 3 is 1.3m. On the other hand, the difference in the flooded area between scenarios 1 and 2 is $62,209.433m^2$ and $57,932.916m^2$. Therefore, the combination of increasing tide and increasing hydrograph is used to do the sensitivity analysis.

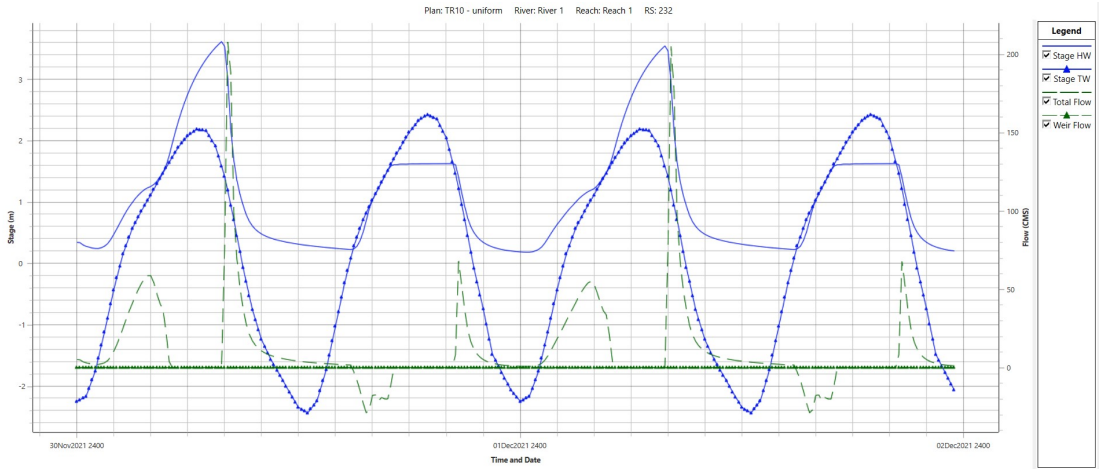

Figure 3.1: Simulation output that represents the stage upstream (blue line) and downstream (blue line with triangles) from gates and total flow through the gates (green line) for increasing hydrograph and tide.

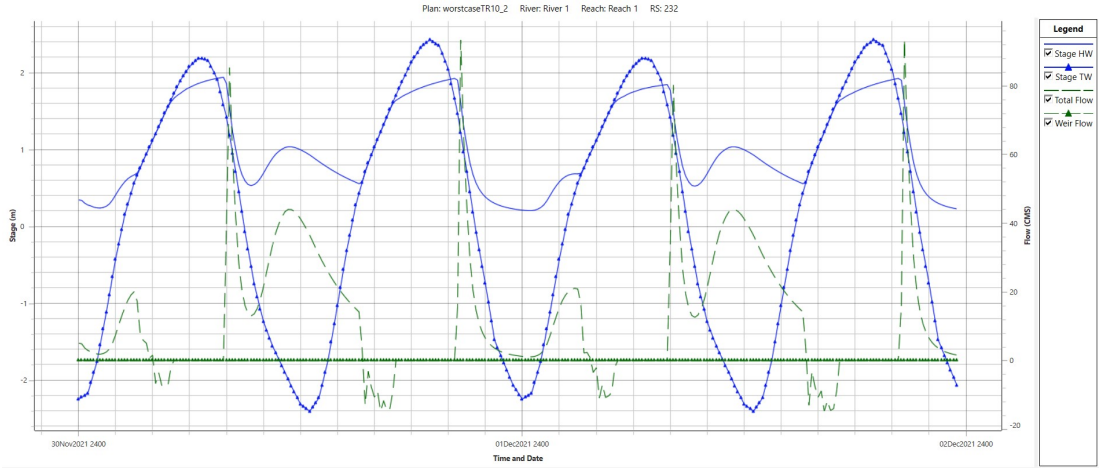

Figure 3.2: Simulation output that represents the stage upstream (blue line) and downstream (blue line with triangles) from gates and total flow through the gates (green line) for increasing hydrograph and decreasing tide.

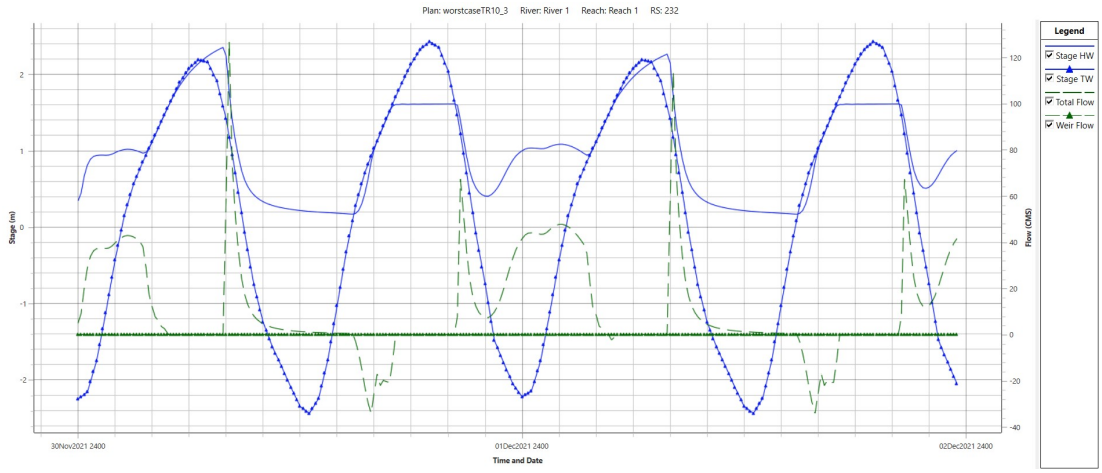

Figure 3.3: Simulation output that represents the stage upstream (blue line) and downstream (blue line with triangles) from gates and total flow through the gates (green line) for increasing tide and decreasing hydrograph.

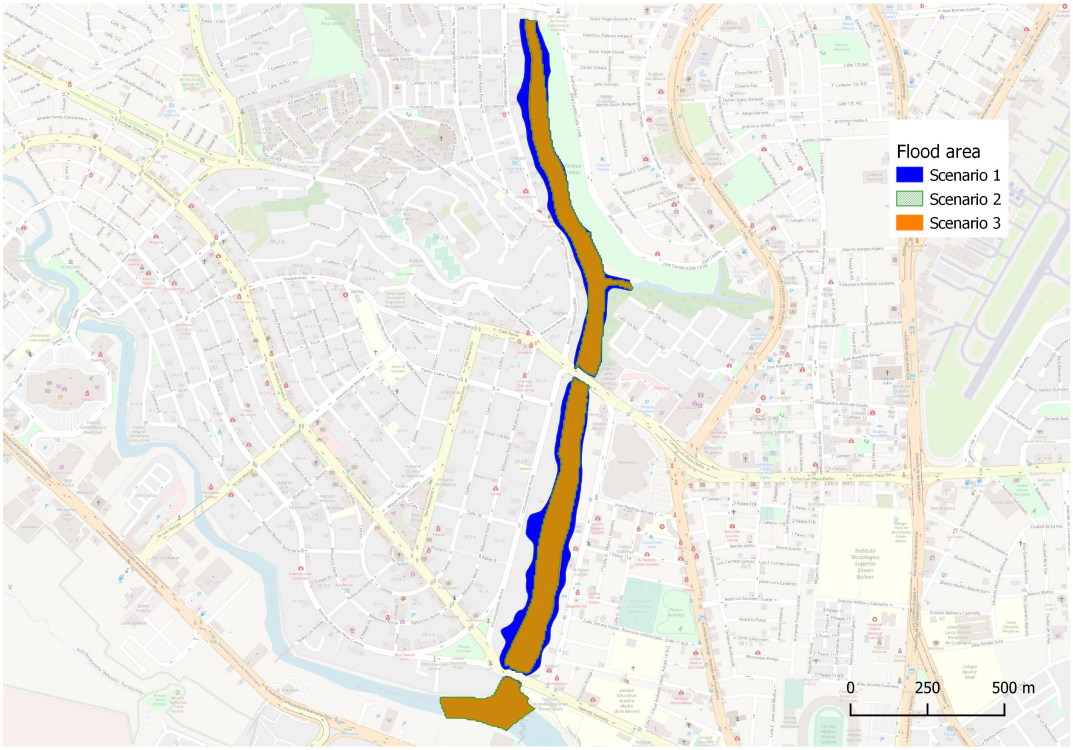

Figure 3.4: Flood area output that represents the worst-case scenario simulation:1) increasing hydrograph and decreasing tide, 2) increasing tide and decreasing hydrograph and 3) increasing tide and decreasing hydrograph.

3.2 Sensitivity analysis

3.2.1 Boundary condition

Water level

In general, the maximum water surface elevation increases when the input hydrograph increases. Figure 3.5 shows the maximum water surface elevation of the hydrodynamic simulation with upstream boundary condition hydrograph of a 2-year return period along the channel, where the water levels reach out $3.22m$ AMSL within the reservoir and $2.43m$ AMSL in the estuary. Similarly, the maximum water surface elevation increases from $3.46m$ for a 5-year return period hydrograph, $3.46m$ (5-year TR), $3.66m$ (10-years TR), $3.90m$ (25-year TR), $4.07m$ (50-year TR) and $4.13m$ with a 100-years return period event (see appendix E). Additionally, with bigger and equal to the 50-year return period event, the reservoir overflows the bridge (gates).

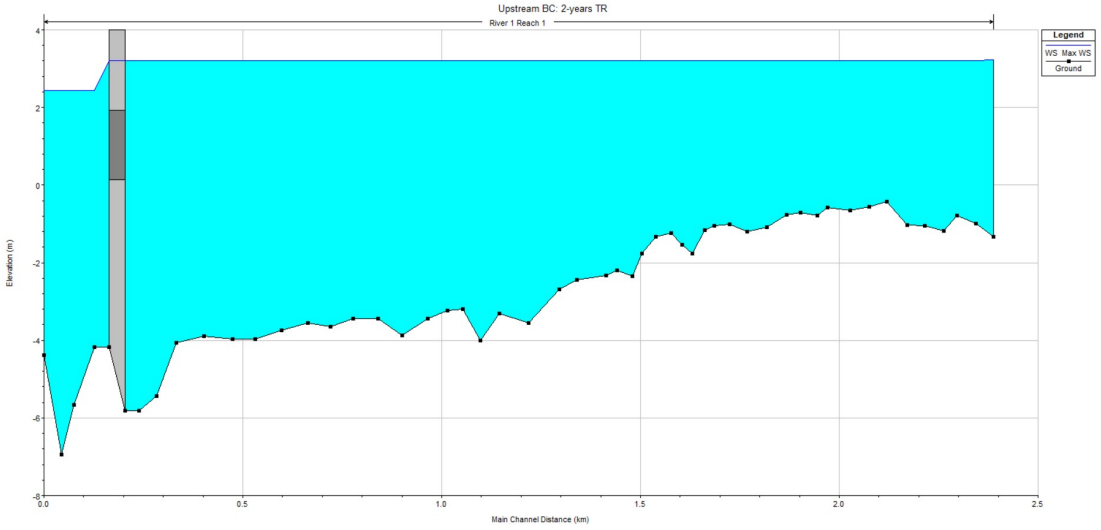

Figure 3.5: Maximum water surface elevation output for a upstream boundary condition of two-years return period hydrograph.

Flood area

Figure 3.6 indicates the extension of the flooded area from the hydrodynamic simulation with different input hydrographs as the upstream boundary condition. For a 2-year event, the flood develops to $19.04ha$, a 5-year event reach to $20.39ha$, $22.16ha$ for 10-year event, $26.88ha$ for 25-year event, $32.48ha$ for 50-year event and $35.21ha$ for 100-year event. Moreover, after a 25-year event, homes could be affected by the water level rise of the reservoir; besides, the upstream rains do not greatly affect the downstream channel.

3.2.2 Hydraulic roughness

Water level

The hydraulic roughness analysis threw values very close to each other. With the default values of the Manning coefficient (main channel = 0.055 and flood plain = 0.12), the maximum water surface elevation reaches $3.65m$ in the reservoir (figure

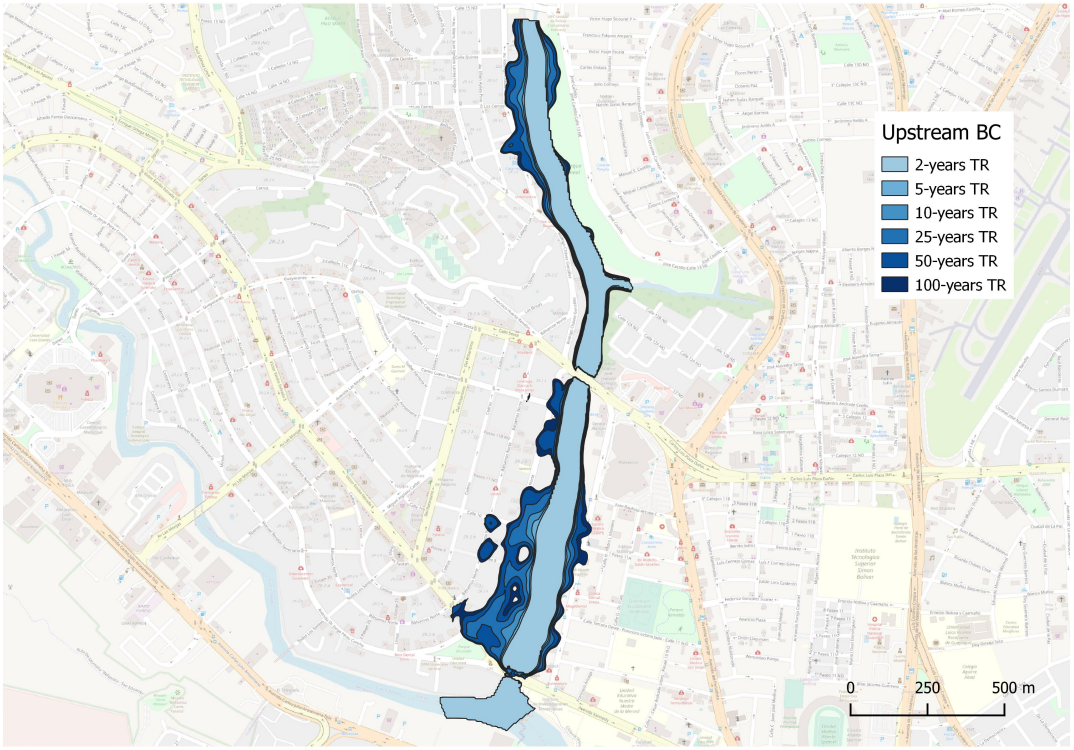

Figure 3.6: Flooding area map for different return period hydrograph (light blue = 2-year TR to dark blue = 100-year TR.

3.7). When the manning values are reduced to 0.044 in the main channel and 0.096 in the flood plain, the water surface elevation attains $3.64m$ (figure E.6). With higher n's values, on the other hand, WSL gets to $3.67m$ (figure E.7). In any Manning coefficient simulated, the water overflow the grates.

Flood area

In the same way, the flooded area is not significantly affected by the change in hydraulic roughness. With a combination of Manning's number of 0.044 for the main channel and 0.096 for the flood plain, the flood extent is 22.06 ha and 22.16 ha for Manning's values of 0.055 and 0.12 in the main channel and flood plain, respectively. Finally, with higher manning values (main channel = 0.066, flood plain = 0.144) water reaches an extension of 22.29 ha (Figure 3.8). According to flood maps, any Manning coefficient simulated directly affects households.

3.2.3 Time step

Water level

The maximum water surface levels vary depending on the time steps used in the simulation. According to the default modelling (Figure 3.9: 10-year TR input hydrograph, Manning coefficient of 0.055 for the main channel and 0.12 for the floodplain and **1-minute time step**), the maximum water level reached in the reservoir is 3.65m AMSL. With shorter time steps, the maximum water surface levels change almost imperceptibly; for example, in the simulation carried out with a time step of 5 seconds, the water levels in the reservoir reach heights

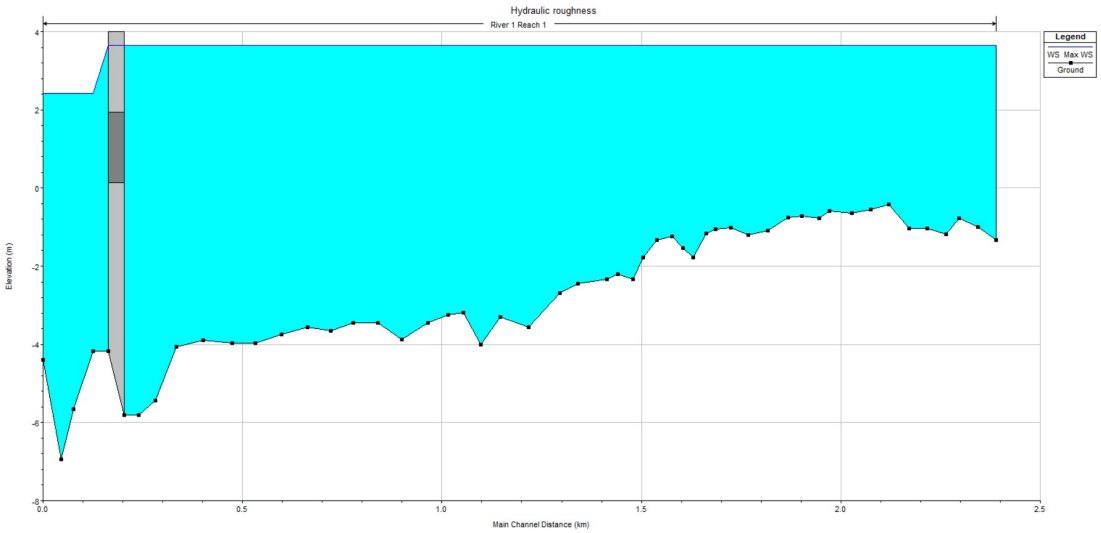

Figure 3.7: Maximum water surface elevation output for a upstream boundary condition of ten-years return period hydrograph, main channel roughness = 0.055 and flood plain roughness = 0.12.

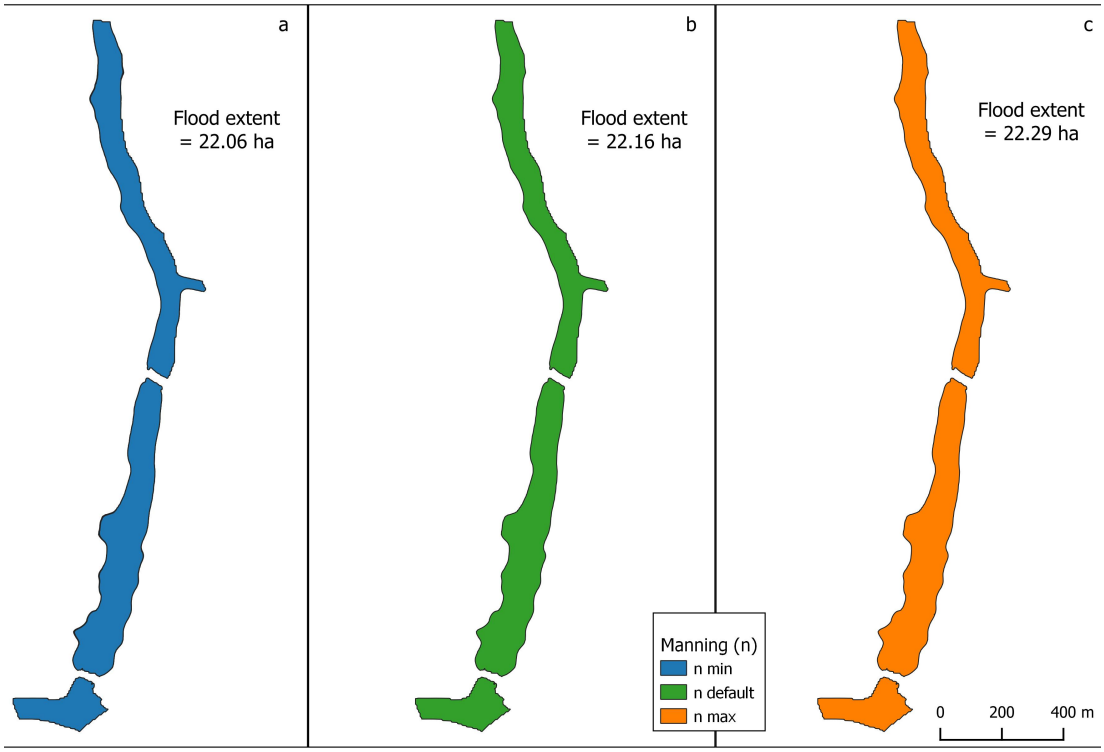

Figure 3.8: Flooding area map for an upstream boundary condition of ten-year return period hydrograph and different hydraulic roughness. a) main channel roughness = 0.044 and flood plain roughness = 0.096, b) main channel roughness = 0.055 and flood plain roughness = 0.12 and c) main channel roughness = 0.066 and flood plain roughness = 0.144.

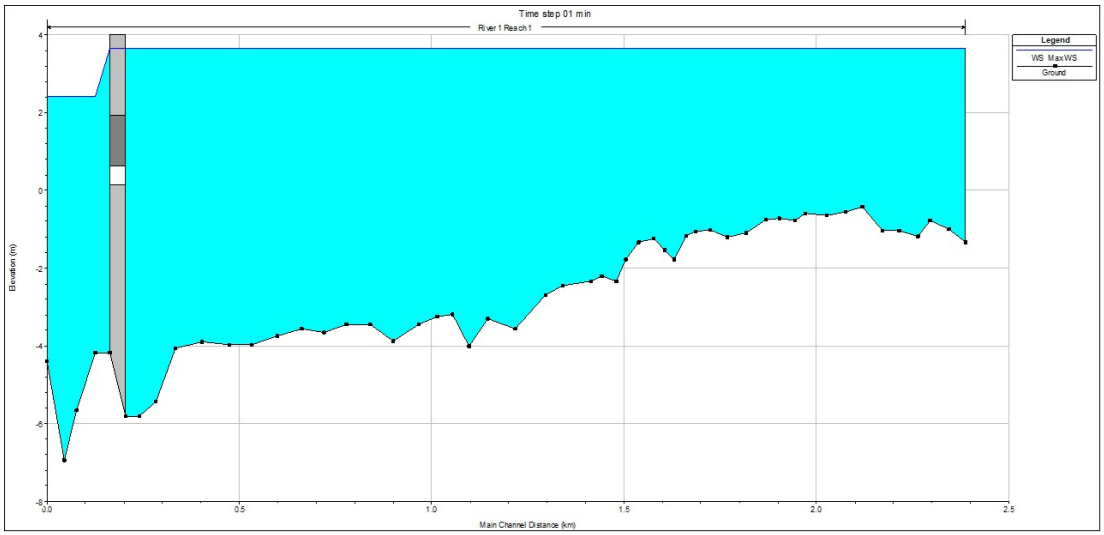

Figure 3.9: Maximum water surface elevation output for a upstream boundary condition of ten-years return period hydrograph, main channel roughness = 0.066 and flood plain roughness = 0.144, and time step = 1 minute.

between 3.64 to 3.66 m AMSL. A similar behaviour occurs when the numerical model has a time discretisation of 10, 15 and 30 seconds; on the other hand, the water levels reached in the reservoir for a time interval of 5 minutes is 3.63m AMSL and 3.62m AMSL for 10 minutes time step. In contrast to lower time steps, 15 and 30-minute modelling intervals threw values of 3.67 and 3.54 m AMSL respectively (for reference, see E.3).

Flood area

The flooded area product of the simulation with a time step of 1 minute advanced to 22.16 ha (figure 3.10). The change in the flooded area when the time step is reduced to 30 seconds changes minimally to 22.17 ha, while when the time step is 5 and 15 seconds, the wet area is 22.21 ha; yet with a 10-second time step, the total flooded area is 22,197 ha. In contrast to low time steps, the larger time steps have slightly more change in the flooded area, that is, reducing concerning 1-minute time steps to 21.8, 21.88 and 21.13 ha for 5-, 10- and 30-minute time steps. The 15-minute time step simulation threw a total inundated area of 22.43 ha.

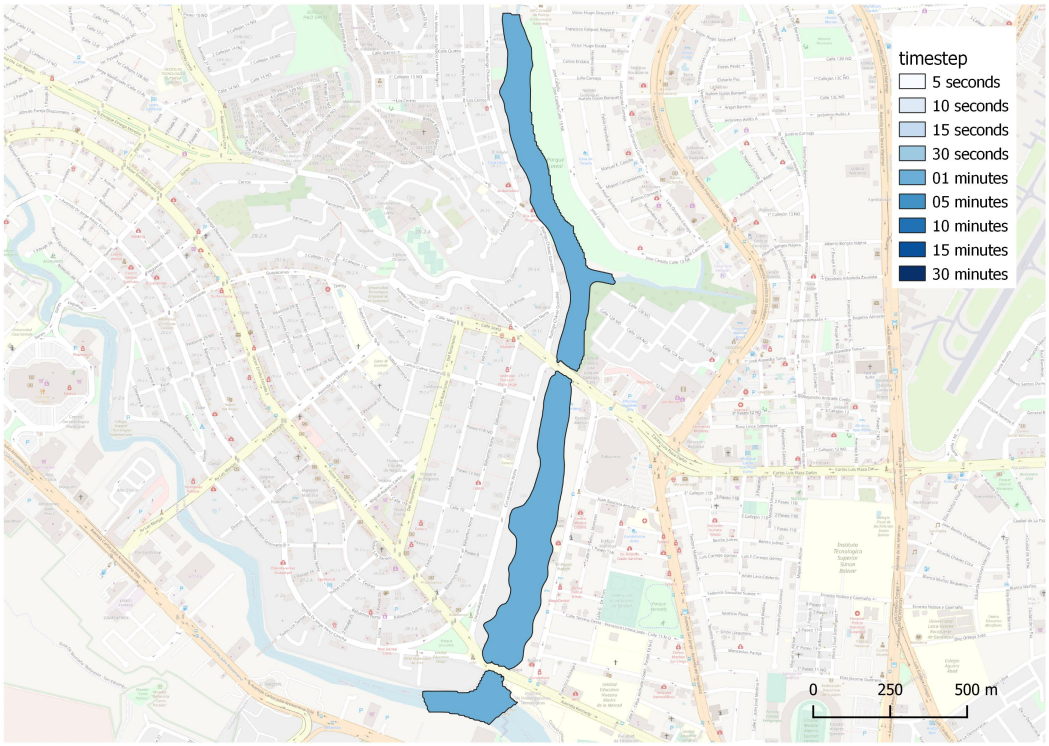

Figure 3.10: Maximum flooded area map output for a upstream boundary condition of ten-years return period hydrograph, main channel roughness = 0.066 and flood plain roughness = 0.144, and time step = 1 minute.

4 Discussion

4.1 Worst case scenario

Constructing a hydrodynamic model entails vast data collection and previous analysis. The lack of information in developing regions, such as Guayaquil, makes this "titanic" work tough, and in some cases, the obtained results are not the most suitable. This project implemented several assumptions following previous works and expert criteria (Ballari et al., 2018; Matamoros et al., 2020; Quichimbo-Miguitama et al., 2022). Thus, the hydrological analysis follows a well-used procedure to calculate the design hydrograph for 2, 5, 10, 25, 50 and 100-year return periods.

Indeed, several combinations of diverse events can affect the study area, which is highly influenced by the tidal and heavy rainfalls. The combination of increasing hydrograph (produced by a storm event) and the increasing tide level can affect the reservoir directly because the tide works as a wall that blocks the normal discharge from the reservoir to the estuary channel. Fortunately, the implementation of 17 valves (gates to the effect of this study) helps to control the tidal inflow to the reservoir, closing with a rate of 0.1 m/min (assumed in the numerical model) when the downstream tide level reaches the 1.5 m AMSL. However, not only the surface water levels are critical but also the velocity peaks (Liu et al., 2019) that exist at the moment of opening the floodgate that may affect the floodgates or the downstream base of the bridge in the future. On the other hand, the other scenarios (rising hydrograph - falling tide and vice versa) allow for rapid release and emptying of the reservoir in more extreme events, which is essential for urban flood management in the city.

In addition to the surface water level, the extent of flooding determined that the most critical scenario is an increased flow and tidal surge simultaneously. Clearly, this is because the reservoir begins to accumulate water and cannot discharge freely into the estuary branch. Thus, the first scenario floods approximately 22.16 ha, while the second scenario only floods 14.94 ha and the third 16.37 ha, a 28% and 26% reduction, respectively, over the first scenario.

4.2 Sensitivity analysis

4.2.1 Boundary condition

Suppose the scenario of a 2-year return period hydrograph is taken as a reference. In that case, it can be seen that as the magnitude of the inflow hydrograph increases, the maximum level of the water surface also increases. This growth is expected (Abdessamed & Abderrazak, 2019; Khalfallah & Saidi, 2018; Romali et al., 2018) and is shown to be constant with the first design hydrographs as follows: $TR5 > 7\%$, $TR10 > 13\%$, $TR25 > 20\%$, $TR50 > 25\%$ and $TR100 > 27\%$ concerning the TR2 event. Also, we can observe the surface water level does not increase significantly between a 50-year and a 100-year event; due to these flows, the water overflows the reservoir both downstream and to the sides of the channel, affecting houses on the reservoir banks (figure 4.1).

In addition to the water level increase in the reservoir, the flooding stain spreads

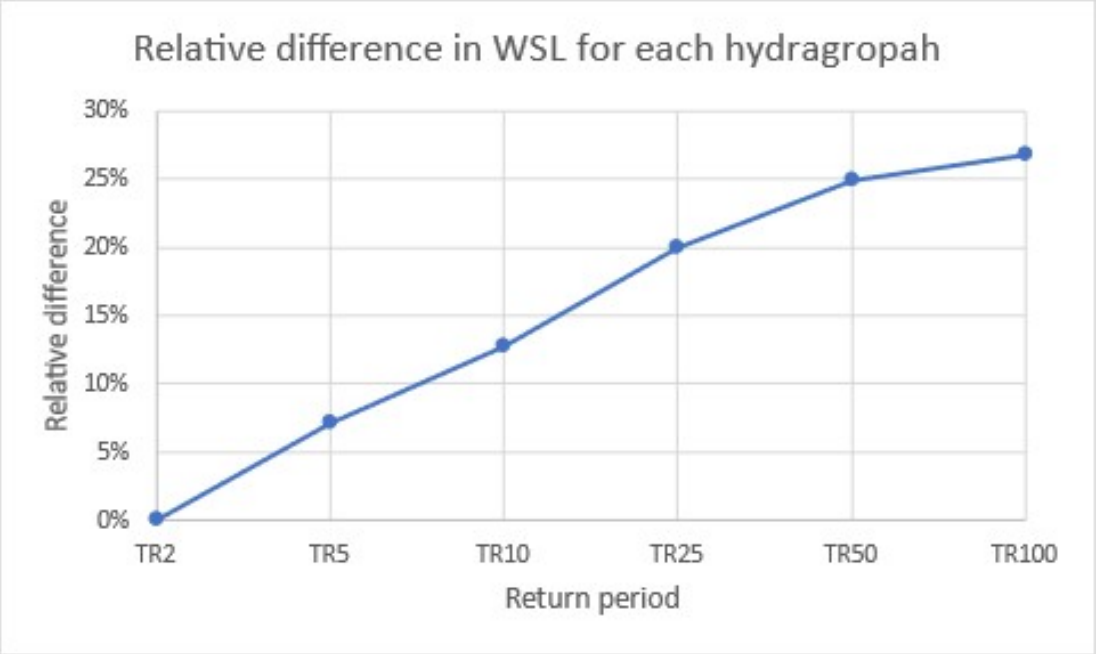

Figure 4.1: Relative error in water surface elevation for each hydrograph

with the increase of design hydrographs. Although there is an inundation of 19.04 ha with a 2-year event, the floodplain increases by 7% with a 5-year event and 16% with a 10-year event. Surprisingly, the reservoir exceeds its capacity and floods its margins by 26.88 and 32.48 ha for events of 25 and 50 years; this threatens the population's homes along the reservoir's banks. Finally, in a 100-year event, the flood spot increases by 85% compared to a 2-year event (figure 4.2).

It is logical to think that the higher the inflow rates, the higher the surface water levels and the wetted area. However, it must be considered that the geometry of the reservoir limits the rise of WSL; once the water levels reach the margins of the reservoir, it will flow into the plains so the WLS variable does not increase as fast as the flooded area.

4.2.2 Hydraulic roughness

Hydraulic roughness is considered one of the most sensitive parameters in hydrodynamic models (Pappenberger et al., 2008). However, under the scenarios modelled in this study, the results with different Manning coefficient values do not differ much from each other. The surface water level does not change even with a difference of 1% for both maximum and minimum values concerning the default values, channel = 0.055 and floodplain = 0.12. Actually, the W.S.L. values increase by only 0.29% with the roughest surface, while it decreases by 0.26% with less rough surfaces (figure 4.3).

Something similar is observed in the extent of flooding, with minimal variations between each scenario. When having rugosities of 0.066 for the main channel and 0.144 for the floodplains, the flood extent is 0.59% larger than the default value (22.16 ha). For Manning's roughness of 0.044 in channels and 0.096 in the channel margins, the flood extent decreased to 0.45% less (figure 4.4).

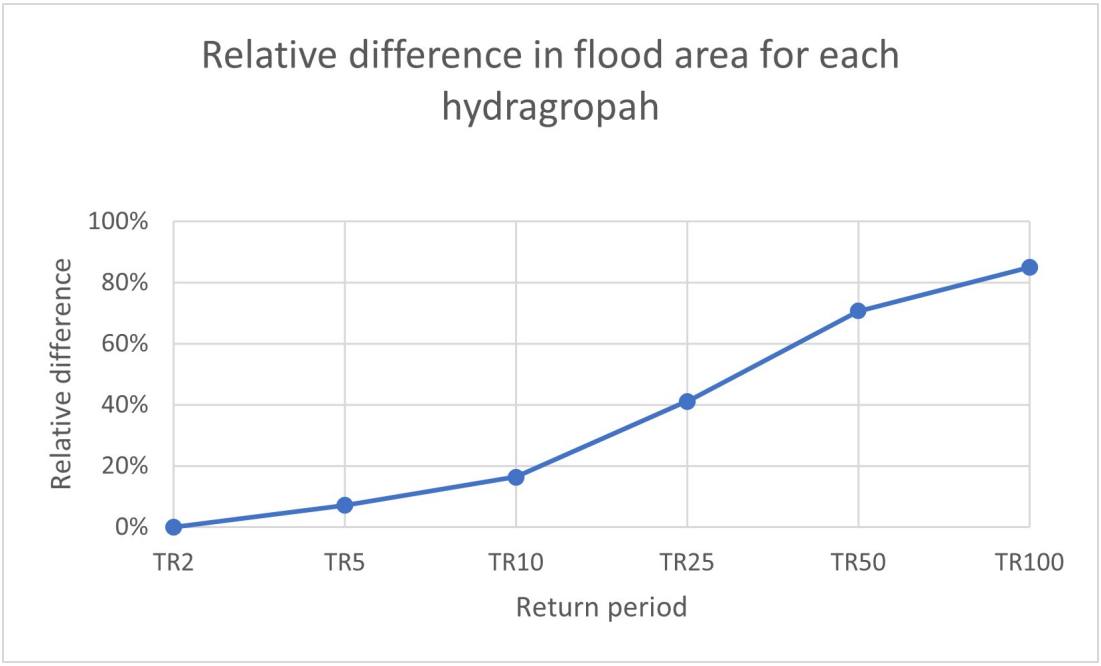

Figure 4.2: Relative error in flood area for each hydrograph

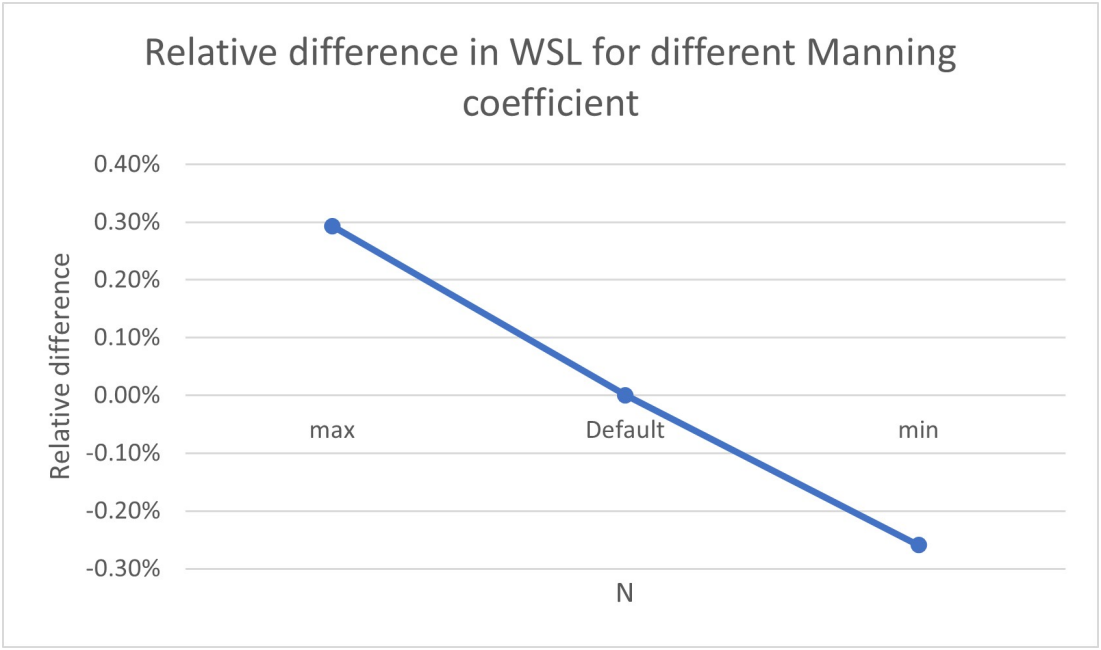

Figure 4.3: Relative error in water surface elevation for each Manning's coefficient

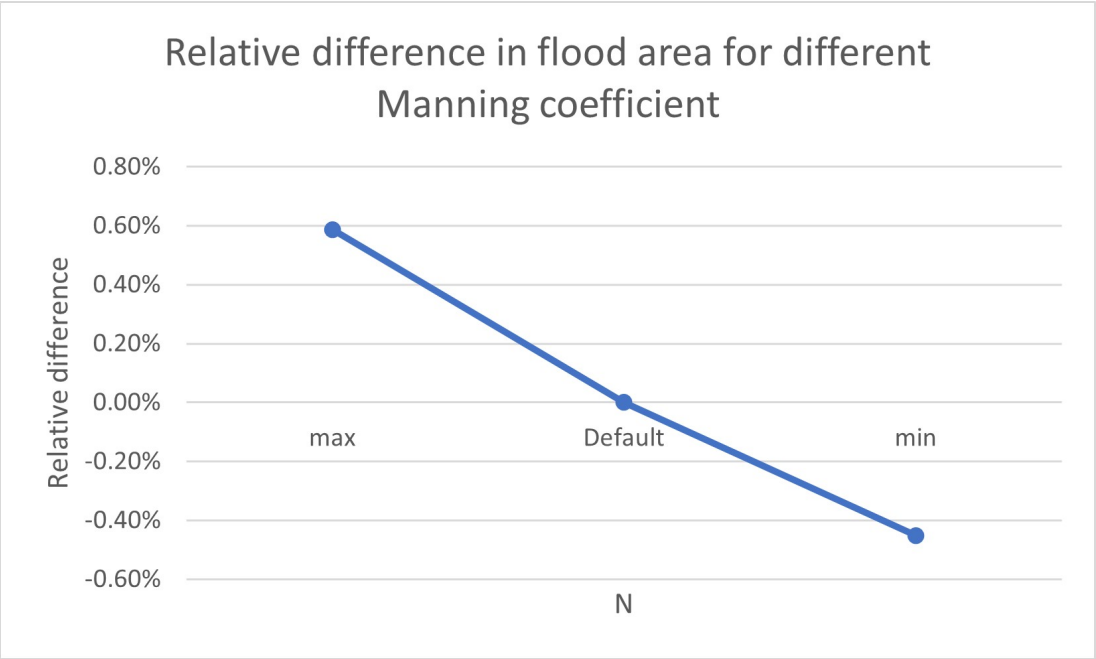

Figure 4.4: Relative error in flood area for each Manning's coefficient

4.2.3 Time step

The base simulation configuration used in the sensitivity analysis for different time steps was a TR10 hydrograph, Manning coefficient 0.055 and 0.12 for the channel and the floodplain, respectively and a time interval of 1 minute. When this scenario is compared with others with shorter time steps, the W.S.L. are not greatly affected by the change in the temporal discretization of the model less than that established in the baseline scenario, that is, the WSL change less than 0.2% (no more than 4 mm). On the other hand, if the time interval increases, the model begins to experience different values in WSL. For example, for time steps between 5 and 15 minutes, the difference is around 1%. In the extreme case of the 30-minute times step, the W.S.L. values decrease by more than 4%. Additionally, instability and errors also increase with high-time steps.

The values of flooding extent remain very similar for the simulations with 5, 10, 15, 30 seconds and 1 minute. These values do not differ by more than 0.22% (percentage given between 1-min and 5-sec model). With time step values greater than 1 minute, on the other hand, the values of flood area differ from each other; for example, for a simulation with a 5 min time interval, the flooded area is reduced by 0.82%, for 10 min the model still gives lower results by 1.25%. Then, modelling with a 15 min time interval gives 22.43 ha flooded, i.e. 1.23% more than the base model. Finally, in a 30-minute time step simulation, the flood values shoot up to 21.13 ha, a difference of 4.67% for the base model (figure 4.5).

The time step sensitivity analysis gives us an important idea of how to optimise the hydrodynamic model, taking into account that the larger the time step, the faster the simulation and that instabilities increase with larger time steps. In this sense, the time step of 1 minute is large enough to have a fast simulation and low enough not to have large instabilities and/or errors (figure 4.6).

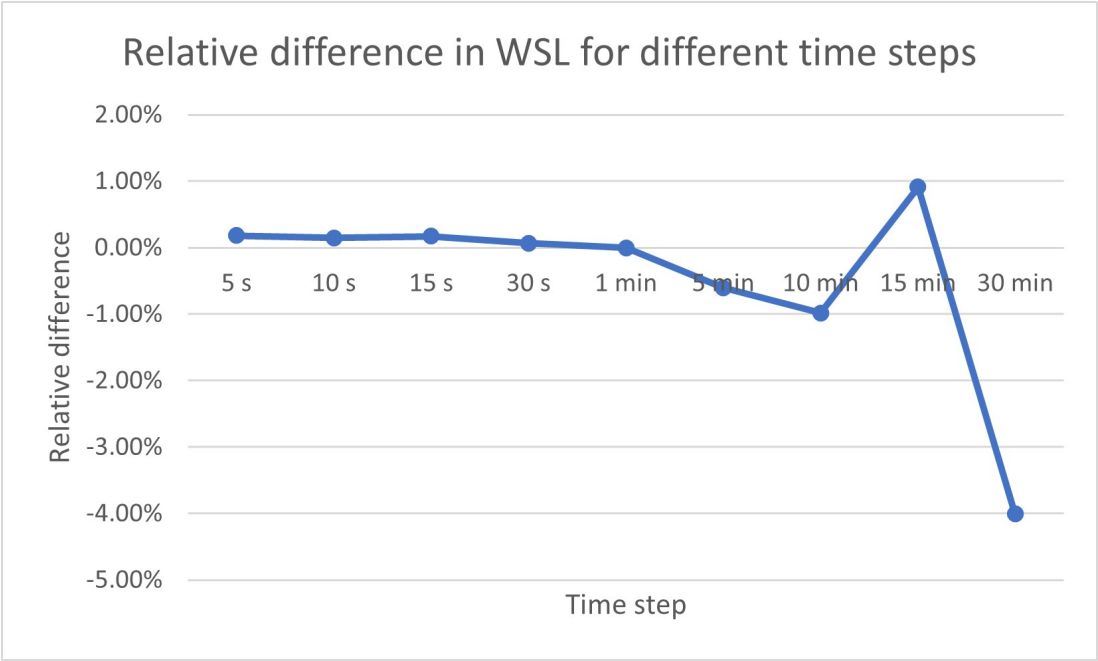

Figure 4.5: Relative error in water surface elevation for each Time step

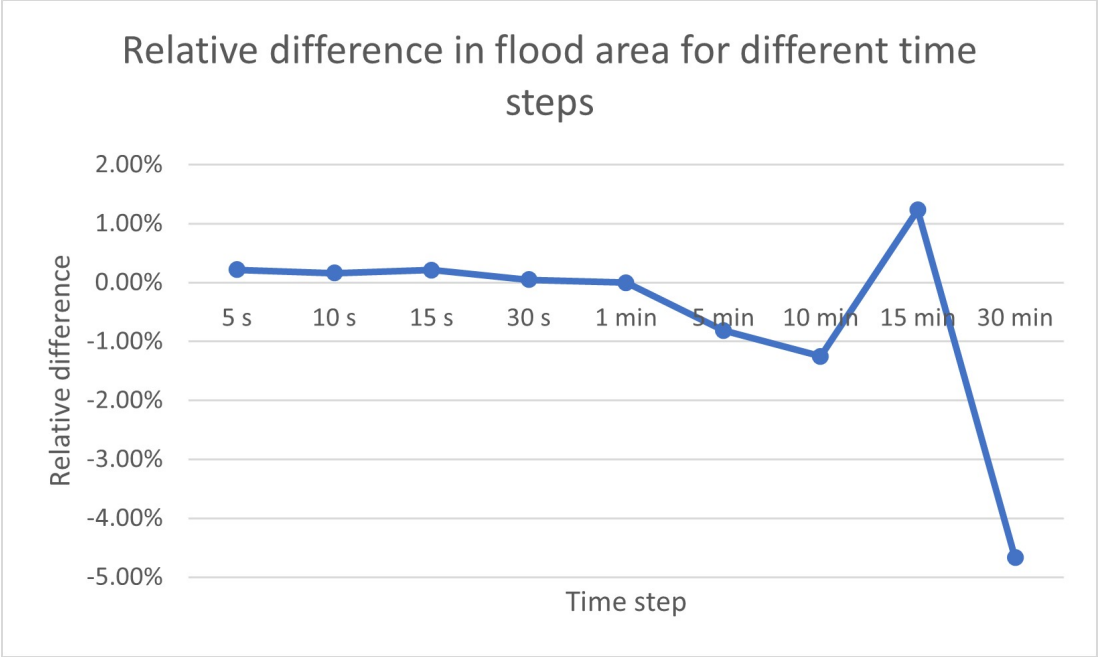

Figure 4.6: Relative error in flood area for each Time step

4.2.4 Model limitations

Despite the key results of this study, it is essential to point out the model's limitations, particularly the lack of relevant data for more robust model construction. Perhaps the total length of the analysed channel may hide interesting patterns determined by the confluence of other estuarine branches. Also, the lack of field-measured data for the calibration and validation process, e.g. water levels within the reservoir, valve outflows or inflows in a given event, leads to increased model uncertainty. In addition, the dispersion of information in different formats makes the synthesis of information in the model complex and prone to errors. This is the case for bathymetry that was taken from two different sources and was in two different references, mean sea level - MSL (reservoir) and mean low water level - MLW (estuary), and although it was possible to bring the data to the same reference level, this carries errors and can lead to a different perception in the model results. In addition to the above, the hydraulic roughness used in this model, although it obeys the interpretation of the images, does not perhaps involve the entire landscape surrounding the study area, such as the mangroves and their aerial roots.

The current system in which the channel is developed has discharges from the stormwater system. Although this lateral flow was implemented in the model with the assumption of uniform lateral flow, it is anticipated that it does not capture how the pipes may involve additional storage space. Additionally, the actual mechanism of the valves differs from those implemented in the model; that is, the check valves (2) only allow the flow from the reservoir to the estuary branch, while the pinch valves (15) allow the inflow and outflow to and from the reservoir; Finally, the latter are completely closed when the downstream tide reaches a certain level. In the model, on the other hand, this mechanism is impossible to implement; for this reason, the 17 valves (check and pinch) close when the downstream tide level reaches 1.5m.

4.2.5 Future uses and improve

Numerical models are a key tool for managing water resources; this is not only limited to the hydrodynamic study of bodies of water but also to chemical and biological behaviour and social behaviour. The estuarine ecosystem is susceptible to sudden changes in its hydrology, and it needs a constant exchange of fresh and saline water to keep its ecosystem regulated. Thus, this model can be improved to determine the ecological implication of blocking the normal tide flow from the estuary to the reservoir. Additionally, the study area must be extended to the neighbouring channels and thus capture the behaviour of the tides in the surrounding channels. With this, it would also be possible to obtain surface runoff from the sector and start efficient management plans in the city.

Urban basins are usually complex systems where buildings, underground infrastructure, and soil types interact. After correct data collection, this model can be improved by capturing the drainage system contribution and the change in land use according to the current state or city planning. An interesting additional application is modelling the effects of climate change or extreme events such as El Niño represented by sea levels rising, and longer rainfalls.

5 Conclusion

The previous hydrological analysis was carried out under several assumptions, such as base flow, curve number, and initial losses. As a result of these assumptions, the hydrological simulation should have been calibrated and validated, yet this step was omitted due to the lack of relevant data. However, when comparing the hydrodynamic model results, it can be inferred that the hydrographs generated in HEC-HMS are quite consistent with reality since, from historical data, it is known that the reservoir has only overflowed with extreme rainfall (e.g. El Niño of 1997-1998) where it rained for more than 600 mm in March accompanied by a rise in sea level.

According to the results obtained to find the worst scenario, the combination of a hydrograph and the rising tide is the most critical for the system; this combination is more severe when the upstream flows are equal to or greater than a 50-year event since it produces an overflow of the bridge that can lead to the failure of the structure. However, using valves that control the inflow of the tide towards the reservoir produces that its capacity remains operational even at high tide. This advantage should be used by the city for better flood management.

From the hydrodynamic simulation, changes in the boundary conditions have a much greater impact on maximum water levels and flood extent than other physical or computational parameters like roughness or time step. Given that growth is ongoing, water levels and floods will continue to rise in response to increasingly catastrophic events. Even though the effect of roughness was not a deciding factor in this study, caution must be taken when selecting this parameter, and it is always advisable to perform a sensitivity analysis and final calibration because, in other studies, Manning's coefficient affects the model's stability as well as its results. The modelling's time step size might also be essential for accuracy and computational stability. While it is true that the model may be more stable at a smaller time step, the amount of processing power required rises; as a result, larger numerical models need either more computing time or even more powerful equipment. The best time step, which provides steady results without error carryover, is one minute, according to the results attained and the condition of this investigation.

6 Bibliography

References

Abdessamed, D., & Abderrazak, B. (2019). Coupling hec-ras and hec-hms in rainfall–runoff modeling and evaluating floodplain inundation maps in arid environments: Case study of ain sefra city, ksour mountain. sw of algeria. *Environmental Earth Sciences*, *78*. https://doi.org/10.1007/s12665-019-8604-6

Armijos, M. M., & Montolío, T. S. (2008). *Ecosistema guayas (ecuador), medio ambiente y sostenibilidad*. Octubre.

Ballari, D., Giraldo, R., Campozano, L., & Samaniego, E. (2018). Spatial functional data analysis for regionalizing precipitation seasonality and intensity in a sparsely monitored region: Unveiling the spatio-temporal dependencies of precipitation in ecuador. *International Journal of Climatology*, *38*, 3337–3354. https://doi.org/10.1002/joc.5504

Barrera Crespo, P. D., Mosselman, E., Giardino, A., Becker, A., Ottevanger, W., Nabi, M., & Arias-Hidalgo, M. (2019). Sediment budget analysis of the guayas river using a process-based model. *Hydrology and Earth System Sciences*, *23*(6), 2763–2778. https://doi.org/10.5194/hess-23-2763-2019

Bhattacharya, A. K., McEnroe, D. M., Zhao, D., Kumar, D., & Shinde, S. (2012). *Modclark model: Improvement and application* (7). www.iosrjen.orgwww.iosrjen.org

Crespo, P. D. B. (2016). *Delft3d flexible mesh modelling of the guayas river and estuary system in ecuador*. http://repository.tudelft.nl/.

Cunderlik, J., & Simonovic, S. P. (2004). *Cfcas project: Assessment of water resources risk and vulnerability to changing climatic conditions*.

Duque-Sarango, P., Patino, D. M., & Lopez, X. E. (2019). Evaluation of the hydrological modeling system hec-hms for the hydrological simulation of a tropical andean micro-basin. *Informacion tecnologica*, *30*, 351–362. http://www.scielo.cl/scielo.php?script=sci_arttext&pid=S0718-07642019000600351&nrm=iso

Easterling, D., Rusticucci, M., Semenov, V., Alexander, L. V., Allen, S., Benito, G., Cavazos, T., Nicholls, N., Easterling, D., Goodess, C., Kanae, S., Kossin, J., Luo, Y., Marengo, J., McInnes, K., Rahimi, M., Reichstein, M., Sorteberg, A., Vera, C., ... Midgley, P. (2012). *3 - changes in climate extremes and their impacts on the natural physical environment*. Cambridge University Press.

Fairchild, T. P., Bennett, W. G., Smith, G., Day, B., Skov, M. W., Möller, I., Beaumont, N., Karunarathna, H., & Griffin, J. N. (2021). Coastal wetlands mitigate storm flooding and associated costs in estuaries. *Environmental Research Letters*, *16*. https://doi.org/10.1088/1748-9326/ac0c45

Garba, H., Ismail, A., & Oriola, F. O. P. (2013). Calibration of hydrognomon model for simulating the hydrology of urban catchment. *Open Journal of Modern Hydrology*, *03*, 75–78. https://doi.org/10.4236/ojmh.2013.32010

INEC. (2017). *Guayaquil en cifras*. Retrieved October 6, 2017, from http://www.ecuadorencifras.gob.ec/guayaquil-en-cifras/

Johnson, F., White, C. J., van Dijk, A., Ekstrom, M., Evans, J. P., Jakob, D., Kiem, A. S., Leonard, M., Rouillard, A., & Westra, S. (2016). Natural hazards in australia: Floods [Floods are caused by a number of interacting factors, making it remarkably difficult to explain changes in flood hazard. ¡br/¿¡br/¿]. *Climatic Change*, *139*, 21–35. https://doi.org/10.1007/s10584-016-1689-y

Khalfallah, C. B., & Saidi, S. (2018). Spatiotemporal floodplain mapping and prediction using hec-ras - gis tools: Case of the mejerda river, tunisia. *Journal of African Earth Sciences*, *142*, 44–51. https://doi.org/10.1016/j.jafrearsci.2018.03.004

Kharb, A., Bhandari, S., de Almeida, M. M., Delgado, R. C., González, P. A., & Tubeuf, S. (2022). *Valuing human impact of natural disasters: A review of methods*. https://doi.org/10.3390/ijerph191811486

Kozanis, S., & Mamassis, N. (2010). Hydrognomon-open source software for the analysis of hydrological data peer review-editorial issues view project european geosciences union general assembly 2013-ntua civil engineering team view project. https://doi.org/10.13140/RG.2.2.21350.83527

Kvočka, D., Falconer, R. A., & Bray, M. (2016). Flood hazard assessment for extreme flood events. *Natural Hazards*, *84*, 1569–1599. https://doi.org/10.1007/s11069-016-2501-z

Lechowska, E. (2018). What determines flood risk perception? a review of factors of flood risk perception and relations between its basic elements. *Natural Hazards*, *94*, 1341–1366. https://doi.org/10.1007/s11069-018-3480-z

Liu, P., Liu, Y., Huang, Z., Cai, B., Sun, Q., Wei, X., & Xin, C. (2019). Design optimization for subsea gate valve based on combined analyses of fluid characteristics and sensitivity. *Journal of Petroleum Science and Engineering*, *182*. https://doi.org/10.1016/j.petrol.2019.106277

Lotze, H. K., Lenihan, H. S., Bourque, B. J., Bradbury, R. H., Cooke, R. G., Kay, M. C., Kidwell, S. M., Kirby, M. X., Peterson, C. H., & Jackson, J. B. (2006). Depletion degradation, and recovery potential of estuaries and coastal seas. *Science*, *312*, 1806–1809. https://doi.org/10.1126/science.1128035

Matamoros, D., Arias-Hidalgo, M., del Pilar Cornejo-Rodriguez, M., & Borbor-Cordova, M. J. (2020). Hydrodynamic analysis of a stormwater system, under data scarcity, for decision-making process: The duran case study (ecuador). *Sustainability (Switzerland)*, *12*, 1–16. https://doi.org/10.3390/su122410541

Molenaar, F., Pak, T., Pous, H. D., & Werff, B.-J. V. D. (2018). *Flood prevention guayaquil a feasibility study on local stormwater storage and the effect of sea branch closure to prevent pluvial and coastal looding multidisciplinary project*. http://repository.tudelft.nl/.

Ongdas, N., Akiyanova, F., Karakulov, Y., Muratbayeva, A., & Zinabdin, N. (2020). Application of hec-ras (2d) for flood hazard maps generation for yesil (ishim) river in kazakhstan. *Water (Switzerland)*, *12*, 1–20. https://doi.org/10.3390/w12102672

Pappenberger, F., Beven, K. J., Ratto, M., & Matgen, P. (2008). Multi-method global sensitivity analysis of flood inundation models. *Advances in Water Resources*, *31*, 1–14. https://doi.org/10.1016/j.advwatres.2007.04.009

Quichimbo-Miguitama, F., Matamoros, D., Jimenez, L., & Quichimbo-Miguitama, P. (2022). Influence of low-impact development in flood control: A case study of the febres cordero stormwater system of guayaquil (ecuador). *Sustainability (Switzerland)*, *14*. https://doi.org/10.3390/su14127109

R. Kabiri, A. C., & Bai, R. (2013). Comparison of scs and green-ampt methods in surface runoff-flooding simulation for klang watershed in malaysia. *Open Journal of Modern Hydrology*, *3*, 102–114. https://doi.org/10.4236/ojmh.2013.33014

Reynaud, J. Y., Witt, C., Pazmiño, A., & Gilces, S. (2018). Tide-dominated deltas in active margin basins: Insights from the guayas estuary, gulf of guayaquil, ecuador. *Marine Geology*, *403*, 165–178. https://doi.org/10.1016/j.margeo.2018.06.002

Romali, N. S., Yusop, Z., & Ismail, A. Z. (2018). Application of hec-ras and arc gis for floodplain mapping in segamat town, malaysia. *International Journal of GEOMATE*, *15*, 7–13. https://doi.org/10.21660/2018.47.3656

Te Chow, V., Maidment, D. R., & Mays, L. W. (1962). Applied hydrology. *Journal of Engineering Education*, *308*, 1959.

Twilley, R. R., Pozo, M., Garcia, V. H., Rivera-Monroy, V. H., & Zambrano, R. (1997). S004420050214. *Oecologia*, *111*, 109–122.

U.S. Army Corps of Engineers, H. E. C. (2012). *Hec-hms hydrologic modeling system, user's manual, version 4.0, cpd-74a*. Hydrologic Engineering Center, Davis, CA.

Valiela, I., Bowen, J. L., & York, J. K. (2001). Mangrove forests: One of the world's threatened major tropical environments. *BioScience*, *51*, 807–815. https://doi.org/10.1641/0006-3568(2001)051[0807:MFOOTW]2.0.CO;2

Vojtek, M., & Vojteková, J. (2016). Flood hazard and flood risk assessment at the local spatial scale: A case study. *Geomatics, Natural Hazards and Risk*, *7*, 1973–1992. https://doi.org/10.1080/19475705.2016.1166874

List of Figures

List of Tables